28415-H002-R0-00

NASA CR-
147828

UTILIZATION OF SOLID-PROPELLANT UPPER STAGES IN STS PAYLOAD ORBITAL OPERATIONS

24 JUNE 1976

Prepared for

NATIONAL AERONAUTICS AND SPACE ADMINISTRATION
LYNDON B. JOHNSON SPACE CENTER

Contract NAS 9-14723

Prepared by S. W. Wilson
S. W. Wilson, Manager
Shuttle/Payload Orbital
Operations Study

Approved by D. K. Phillips
D. K. Phillips, Manager
Systems Engineering and
Analysis Department

Systems Engineering and Analysis Department

TRW

Defense and Space Systems Group

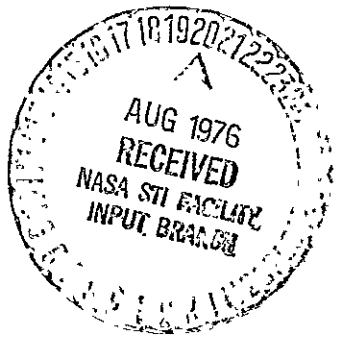

CONTENTS

CONTENTS (Continued)

FIGURES

TABLES

NOMENCLATURE

Symbol	Definition
$\vec{c}$	Orbital transfer chord vector (see Figure 10)
$\hat{c}$	Orbital transfer chord unit vector, $\vec{c}/\lvert\vec{c}\rvert$
c	Orbital transfer chord length, $\lvert\vec{c}\rvert$
e	Orbit eccentricity
f	True anomaly
g	Gravitational acceleration under standard conditions, 32.174 ft/sec^2
i	Orbit inclination relative to equator
$\hat{i}$, $\hat{j}$, $\hat{k}$	Local-vertical unit vectors ($\hat{k} = -\vec{r}/\lvert\vec{r}\rvert$, $\vec{j} = -\vec{r} \times \vec{v}/\lvert\vec{r} \times \vec{v}\rvert$, $\hat{i} = \hat{j} \times \hat{k}$)
$\hat{I}$, $\hat{J}$, $\hat{K}$	Local vertical unit vectors at perigee
I_{SP}	Specific impulse
$\hat{N}$	Unit vector pointing in the direction of a relative node
P	Orbit period
p	Semilatus rectum of orbit
r	Distance from center of earth
$\vec{r}$	Position vector
t	Time
u	Argument of latitude
$\hat{U}$	Unit vector directed toward point of maximum northerly declination in orbit
v	Velocity magnitude
$\vec{v}$	Velocity vector

NOMENCLATURE (Continued)

Symbol	Definition
V	SRM stage ΔV capability
$\vec{V}_G$	Velocity to be gained
$\vec{V}_R$	Required velocity
W	Wedge angle between orbit planes
W_{BO}	Burnout gross weight
W_P	Propellant weight
$\dot{X}$, $\dot{Y}$, $\dot{Z}$	Local-vertical components of velocity ($\dot{X} = \vec{V} \cdot \hat{i}$, $\dot{Y} = \vec{V} \cdot \hat{j}$, $\dot{Z} = \vec{V} \cdot \hat{k}$)
$\overline{X}$, $\overline{Y}$	Scan-control variables
α	Thrust angle relative to $\vec{V}_G$
β	Flight path angle
Δ	Wedge angle between initial and target orbit planes
ΔV	Velocity increment magnitude
$\Delta\vec{V}$	Velocity increment
θ	Transfer angle
λ	Angle between relative node and impulse point
μ	Gravitational parameter of the earth
π	Ratio of circumference to diameter of a circle, 3.14159.....
ω	Argument of perigee
Ω	Right ascension of ascending node on the equator
$\hat{\Omega}$	Unit vector pointing in direction of ascending node

NOMENCLATURE (Continued)

Subscripts

Symbol	Definition
A	Apogee
F	"Free" (unconstrained) impulse point
I	Initial orbit
ℓ, m, n	Indices of particular solutions in cases where multiple solutions are possible
o	Premaneuver condition or condition at a constrained impulse point
P	Perigee
T	Target orbit
X	Transfer orbit
α	Apsidal condition

ACKNOWLEDGMENT

The author is indebted to Mr. J. J. McMahon for checking the equations in this report, and for detecting several algebraic errors that existed in the draft.

1. INTRODUCTION

The Space and Missile Systems Organization of the Department of Defense (DOD) has recently issued a Request for Proposal (RFP) for the design of an Interim Upper Stage (IUS) to be used in conjunction with the Space Shuttle for transporting STS payloads to orbits beyond the Shuttle performance envolope.

The IUS design is to employ expendable solid rocket motors (SRM's) for major translational maneuvers. Although the question is not addressed specifically in the RFP, it is expected that the IUS design will not provide for guidance-commanded SRM thrust termination such as might conceivably be effected by chemical quenching or thrust chamber venting. A summary of probable IUS design characteristics, extracted from the aforementioned RFP, is included in the Appendix.

The main purpose of this report is to discuss techniques of trajectory design, maneuver execution, and stage loading that are compatible with the use of SRM's which, once ignited, must burn to propellant depletion. It is anticipated that some Shuttle payloads will use non-IUS solid propellant kick stages; therefore this subject is also pertinent to Shuttle flights other than those involving the use of the IUS.

The SRM utilization techniques can be divided into two major categories: (1) those in which the stage performance is adjusted to match the ΔV requirements of a preselected trajectory, and (2) those in which the trajectory is designed to match the ΔV capability of the stage(s). These two categories are discussed separately in Sections 2 and 3.

2. ADJUSTMENT OF SRM STAGE PERFORMANCE TO MATCH TRAJECTORY ΔV REQUIREMENTS

Within this category of techniques it is assumed that a nominal trajectory has been selected to deliver a particular payload to a specific orbit and that, for each major velocity impulse, an SRM has been identified which is capable of delivering more than the required ΔV. The problem then is one of reducing the effective ΔV delivered by the SRM stage so as to match the trajectory requirement.

These techniques allow the use of conventional trajectory design methods and software; i.e., those in which velocity impulse magnitudes are not constrained to be equal to specific values. Aside from any question of computational difficulty, it is not desirable to impose equality constraints on the velocity impulses during trajectory design because doing so removes degrees of freedom which may be needed to satisfy environmental or operational constraints.

2.1 STAGE BALLASTING

For a given specific impulse I_{SP}, propellant loading W_P, and burnout gross weight W_{BO}, the ideal velocity increment* that will be delivered by the SRM is uniquely determined by the rocket equation

$$\Delta V_{ideal} = g\, I_{SP}\, \ell n \left(\frac{W_{BO} + W_P}{W_{BO}} \right) . \qquad (1)$$

Ballasting increases the burnout weight W_{BO}, thereby reducing the ΔV capability of the stage. Although useful in some instances, this technique is generally undesirable because it involves a double weight penalty. The weight of the excess propellant and the weight of the ballast necessary to counteract it must both be transported into orbit by the Shuttle.

*The velocity increment that would be realized by thrusting in a fixed direction in gravity-free space.

2.2 PROPELLANT OFFLOADING

The ΔV capability of a given SRM stage can also be reduced by offloading propellant, thereby reducing W_p in Equation (1). Weightwise, this is more efficient than ballasting. The magnitude of the weight advantage over ballasting will depend on whether or not it is necessary to replace the offloaded propellant with inert material so as to maintain the structural integrity of the SRM, which in turn depends mainly on the propellant grain configuration.

A practical problem associated with SRM propellant offloading is that it must be accomplished at the manufacturing facility, well in advance of the flight date. Therefore this technique is intolerant of changes in payload weight or flight objective after the SRM has been assembled.

2.3 POWERED-FLIGHT ATTITUDE MANEUVERS

Neither of the two preceding techniques affords, within themselves, the capability to compensate for trajectory dispersions detected during flight. If the upper stage guidance and control system is capable of controlled attitude maneuvers during the SRM burn, then such compensations can be made by varying the orientation of the thrust vector. Given sufficient maneuverability, gross reductions of the effective SRM ΔV can be attained. The basic idea is to waste the excess ΔV produced by the SRM by thrusting in a "non-optimum" direction. Many variations of this technique are possible; two of the simpler ones are discussed in Sections 2.3.1 and 2.3.2.

2.3.1 Dog-Leg Steering

Figure 1 illustrates the geometry, in inertial velocity space, of the dog-leg maneuver. This is essentially an "external ΔV" maneuver type, in which the objective is to achieve a resultant $\vec{\Delta V}$ vector (as sensed by onboard accelerometers) supplied as a target value by premaneuver computations. Operationally, the SRM thrust line would be aligned with the inertial direction of Leg 1 prior to ignition. After ignition, the thrust direction would be held fixed until the proper time (as determined by accelerometer output) for initiating a constant-rate turn that would align the thrust vector with Leg 2. After achieving proper alignment on Leg 2 (on a bearing that passes through the coordinates of the desired resultant $\vec{\Delta V}$), the thrust direction would again be held inertially fixed until SRM burnout occurred.

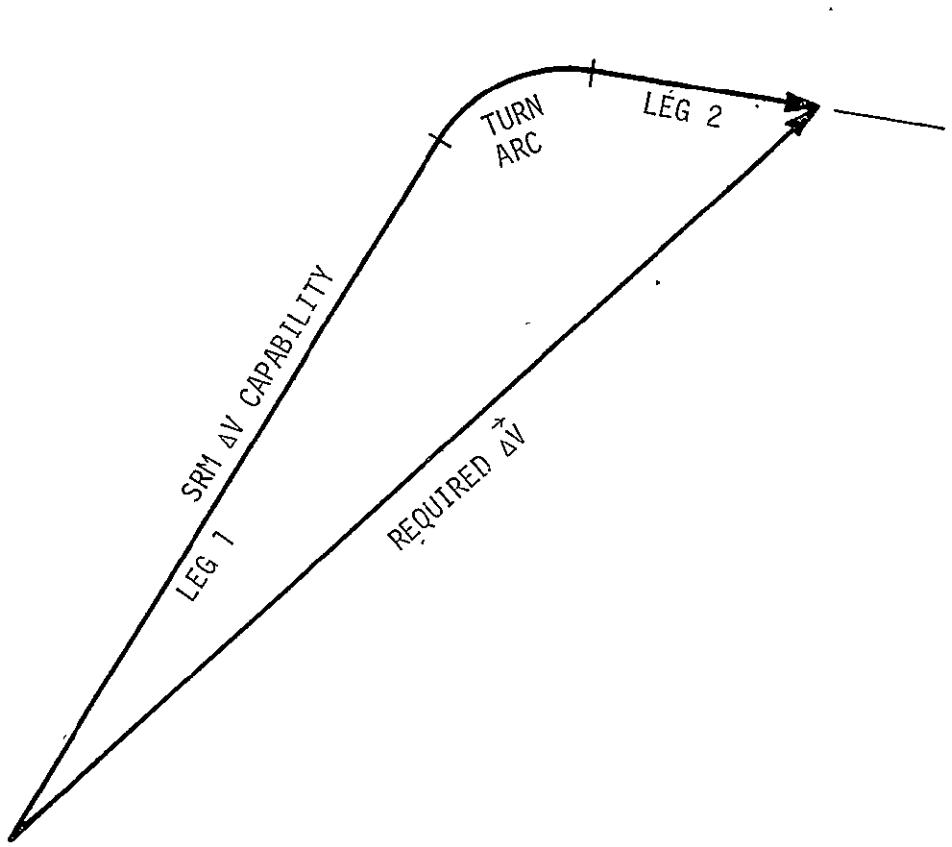

Figure 1. Dog-Leg Steering Geometry

For a given SRM ΔV capability greater than the required resultant ΔV, there are obviously many different combinations of turning rate and Leg 1/ Leg 2 orientation that would nominally achieve the desired result. The turning rate will of course be limited by permissable load factors and by the available directional control authority and control accuracy. Assume for the moment that a rate has been determined. This still leaves open the question of how the direction of Leg 1 or of Leg 2 should be chosen. If the orientation of either leg is specified, the orientation of the other is uniquely determined by the SRM ΔV capability.

Since the total ΔV delivered by the SRM (consequently, the length of Leg 2) will always be uncertain to some extent, it is believed that the best policy for dog-leg steering would be to align Leg 2 with the "least critical direction" in velocity space. By definition, this is the direction in which a velocity variation of a given magnitude will have the smallest possible undesirable effect on the ensuing trajectory. The definition of the least critical direction would depend on the maneuver objective. For instance, if the maneuver were calculated to intercept a moving target, this might be the direction (easily calculable from a state transition matrix or from solution of Lambert's problem) in which a small velocity variation would not cause the target to be missed, but instead would only change the time of intercept. In general, the least critical direction can be defined by the vector cross product of the gradients, in velocity space, of the two most critical postmaneuver trajectory parameters.

2.3.2 Circular-Arc Steering

The geometry of the circular-arc steering algorithm (Reference 1) is illustrated in Figure 2. Unlike the dog-leg method, its use is not restricted to "external ΔV" maneuver types. It can also be used in conjunction with guidance logic in which the required velocity $\vec{V}_R$ is periodically updated during the maneuver (e.g., by Lambert solutions based on the navigation system's estimate of the current state vector). At any instant, the desired angle α between the thrust vector and the velocity-to-be gained vector $\vec{V}_G$ is calculated from the equation

$$\frac{\sin \alpha}{\alpha} = \frac{|\vec{V}_G|}{V} \quad , \tag{2}$$

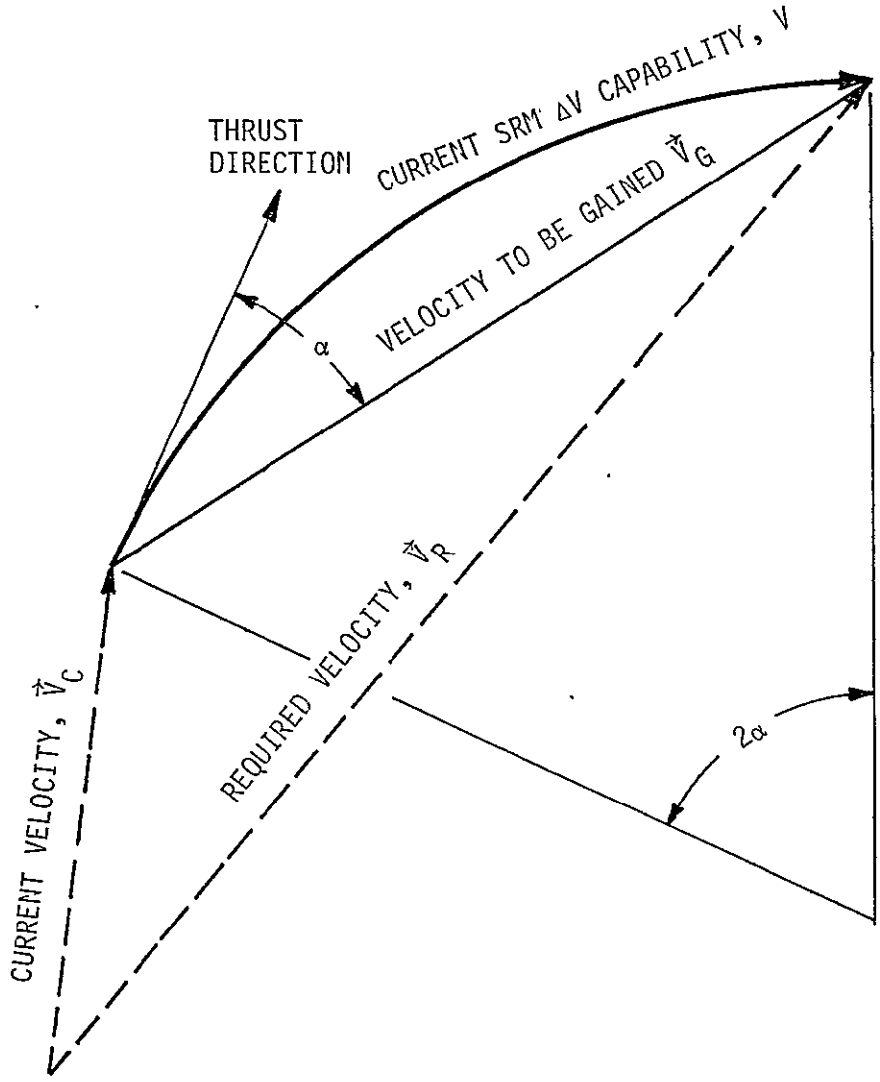

Figure 2. Circular-Arc Steering Geometry

where V is the guidance system's estimate of the remaining ΔV capability of the SRM. As illustrated in Figure 2, V and $|\vec{V}_G|$ correspond to the arc length and chord length, respectively, of a segment of a circle. A potential advantage of this steering policy is that it tends to minimize the turning rate, although in practice it may be necessary to freeze the thrust direction near the end of the burn to preclude excessive rates that could result from underestimating V.

It should be noted that the thrust direction is not completely defined by Equation (2). The steering angle α can be measured in any plane that contains $\vec{V}_G$. And for any permissable plane, either of two opposite angular directions may be chosen. To minimize the deleterious effects of SRM ΔV uncertainties, probably the best policy would be to choose the steering plane and angular direction that would align the burnout thrust vector as closely as possible with the "least-critical" direction discussed in Section 2.3.1.

3. DESIGN OF TRAJECTORIES TO MATCH SRM STAGE ΔV CAPABILITIES

For SRM stages incapable of powered-flight attitude maneuvers, it may be necessary to design trajectories with velocity impulse magnitudes constrained to be equal to specific stage ΔV capabilities. Even if ballasting and/or propellant offloading techniques are used to adjust SRM stage performance to the requirements of a preselected nominal trajectory, such a trajectory design capability may be needed during flight operations so that maneuvers can be retargeted to compensate for dispersions.

In Sections 3.1 through 3.4, various classes of upper-stage maneuver targeting and trajectory design problems are discussed. Emphasis is placed on the nature and types of the solutions that are possible when ΔV magnitudes are constrained to specific values, as deduced from analytical considerations. A conic-impulsive trajectory model, wherein coasting flight segments are approximated by two-body motion and powered flight segments are approximated by instantaneous velocity increments, is used in all cases for analytical purposes. Such a model is adequate in most cases for conceptual design and for feasibility assessment. Analytic solutions based on such modeling are also valuable for high-fidelity precision maneuver targeting. They can serve either to generate "first guesses" for conventional iteration processes that use state transition matrices, or to provide both the first guesses and updated independent variable values (based on trial trajectory integrations) in a recursive iteration loop similar to that described in References 2 and 3.

3.1 SINGLE-IMPULSE ORBIT MODIFICATION

The problem types to be considered in this section are those where it is desired to attain, with a single velocity increment of fixed magnitude, a postmaneuver orbit having specific characteristics. In the general case where the impulse can be applied at any point on the premaneuver orbit, it may be possible to satisfy as many as three mutually independent postmaneuver orbit constraints. However, the discussion in this section will be limited to the restricted case where the maneuver position and the premaneuver velocity are fixed; e.g., by specifying either the time of the impulse or the angular position of the impulse point in the premaneuver orbit. With this

type of restriction there are only two degrees of freedom (represented, say, by two angles that define the direction of the velocity increment), and therefore no more than two mutually independent postmaneuver orbit constraints can be satisfied simultaneously.

For analysis purposes, consider an inertial Cartesian coordinate system in which the Z-axis is oriented in a direction opposite to that of the position vector of the impulse point, the Y-axis is oriented in a direction opposite to that of the angular momentum vector, and the X-axis completes a right hand orthogonal triad. The impulse position and premaneuver vectors can then be represented by

$$\vec{r}_o = - \hat{k}\, r_o \tag{3}$$

and

$$\vec{v}_o = \hat{i}\, \dot{X}_o + \hat{k}\, \dot{Z}_o \quad . \tag{4}$$

As illustrated in Figure 3, the locus of all possible postmaneuver velocity coordinates is represented by the surface of an "SRM capability sphere" in velocity space. The equation of the capability sphere is

$$\left(\dot{X} - \dot{X}_o\right)^2 + \dot{Y}^2 + \left(\dot{Z} - \dot{Z}_o\right)^2 = V^2 \quad , \tag{5}$$

where V represents the magnitude of the velocity increment produced by the SRM, and where the postmaneuver velocity vector is represented by

$$\vec{v} = \hat{i}\, \dot{X} + \hat{j}\, \dot{Y} + \hat{k}\, \dot{Z} \quad . \tag{6}$$

In general, the specification of one postmaneuver orbit constraint defines a surface in velocity space. The specification of two constraints defines one or more curves in velocity space representing the intersection(s) of two surfaces, provided of course that it is physically possible to satisfy the two constraints (i.e., that the constraint surfaces do in fact intersect each other). The maneuver targeting problems discussed in Sections 3.1.1 through 3.1.5 involve geometric solutions to find the points, if they exist, at which such curves intersect the surface of the SRM capability sphere.

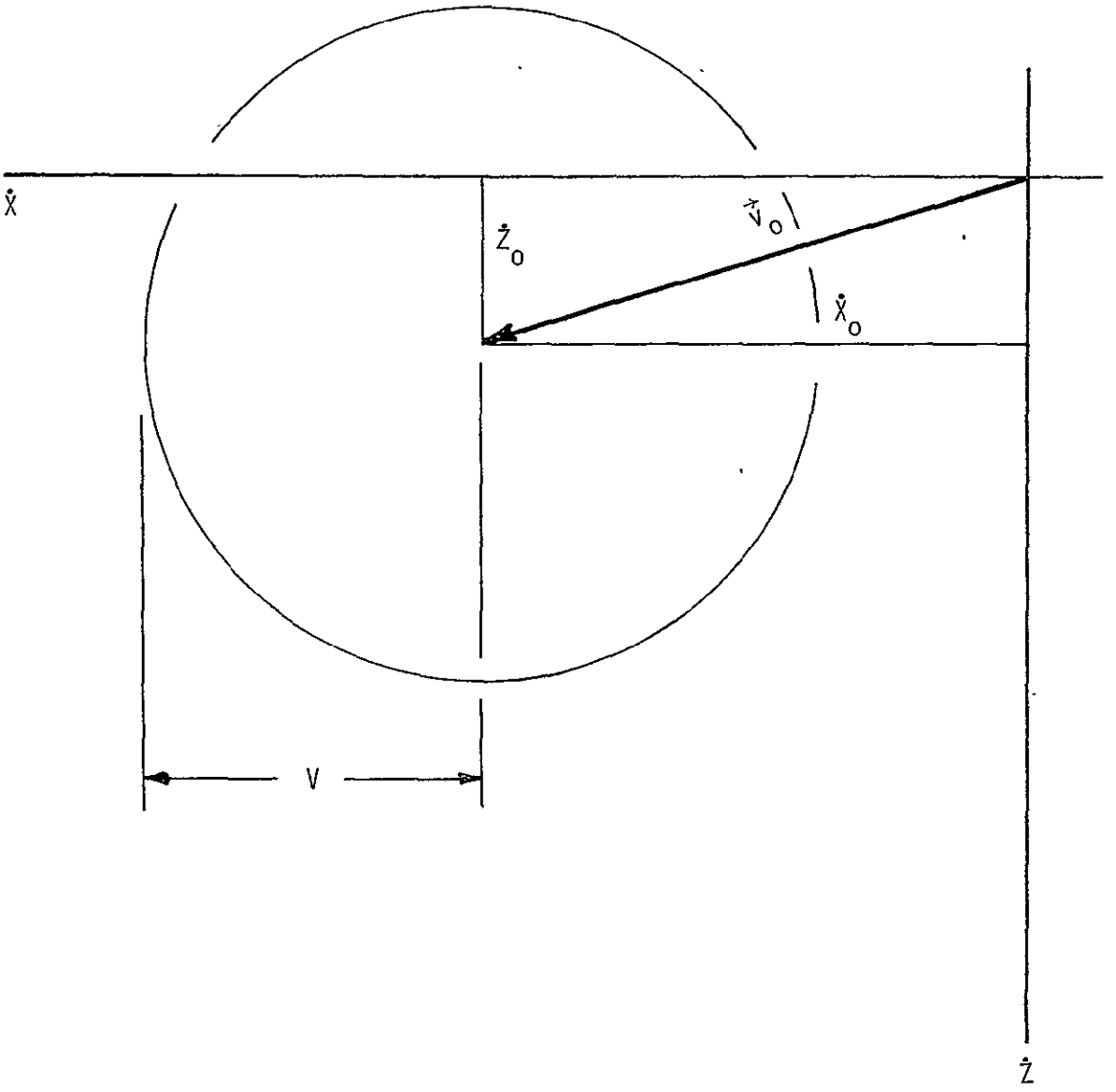

Figure 3. Premaneuver Velocity Vector and SRM Capability Sphere

The problem types to be discussed are representative of those commonly encountered, but by no means do they encompass all possible single-impulse targeting problems.

3.1.1 Orbit Circularization

Requiring the postmaneuver orbit to be circular is the same as requiring the eccentricity e to be zero. In general, assignment of a specific value to e defines a surface in velocity space just as if it were any other scalar orbit parameter. At $e = 0$, however, the constraint surface degenerates into a curve. Specifically, the locus of velocity coordinates that satisfy this constraint is a circle whose equations are

$$\dot{Z} = 0 \tag{7}$$

and

$$\dot{X}^2 + \dot{Y}^2 = \mu/r_o \quad , \tag{8}$$

where μ is the gravitational parameter of the central body. Substituting Equations (7) and (8) into Equation (5) yields the partial solution

$$\dot{X} = \left(\mu/r_o + \dot{X}_o^2 + \dot{Z}_o^2 - V^2\right)/(2\,\dot{X}_o) \tag{9}$$

provided $\dot{X}_o \neq 0$*. The remainder of the solution is found by substituting the numerical value of $\dot{X}$ from Equation (9) into Equation (8) and solving for the two possible values of $\dot{Y}$, thus:

$$\dot{Y}_\ell = \pm\sqrt{(\mu/r_o) - \dot{X}^2} \quad , \tag{10}$$

*If $\dot{X}_o = 0$ (which is unlikely, since it could only occur if the premaneuver velocity vector were either zero or oriented in a vertical direction), then a solution exists only if $\mu/r_o + \dot{X}_o^2 + \dot{Z}_o^2 - V^2 = 0$.

where the subscript ℓ takes on the value 1 when the minus sign is used and the value 2 when the plus sign is used. If the radicand is negative in Equation (10), then of course there is no physical solution to the targeting problem.

In general, the roots of Equation (10) will not be zero. This means than an orbital plane change is generally necessary if the orbit is to be circularized with a velocity increment of fixed magnitude. The magnitude and direction of the plane change is defined by the wedge angle W, where

$$\sin W = \dot{Y} / \sqrt{\dot{X}^2 + \dot{Y}^2} \tag{11}$$

and

$$\cos W = \dot{X} / \sqrt{\dot{X}^2 + \dot{Y}^2} \quad . \tag{12}$$

The wedge angle is positive when the maneuver produces a positive rotation of the orbit plane about the Z-axis.

3.1.2 Achievement of Specified Apogee and Perigee Altitudes

Specifying the altitude of either apsis (apogee or perigee) of the postmaneuver orbit is a special case of a more general type of constraint which requires that the flight path angle β (the angle between the position vector and the velocity vector) have a specific value β_T at a given radial distance r_T from the center of attraction. Since the general form is applicable to other targeting problems (e.g., calculating deorbit maneuvers), the general equation of the constraint surface will be developed before invoking the special conditions that apply to apsis altitude constraints.

For the trivial case where $r_T = r_o$, the constraint surface is that of a cone whose equation is

$$\dot{Z}^2 \sin^2 \beta_T = (\dot{X}^2 + \dot{Y}^2) \cos^2 \beta_T \quad . \tag{13}$$

For the non-trivial case (i.e., where $r_T \neq r_o$), the conservation of energy and angular momentum requires that

$$\dot{X}^2 + \dot{Y}^2 + \dot{Z}^2 - 2\mu/r_o = v_T^2 - 2\mu/r_T \tag{14}$$

and that

$$r_o^2 (\dot{X}^2 + \dot{Y}^2) = r_T^2 v_T^2 \sin^2 \beta_T \quad , \tag{15}$$

where v_T is the velocity magnitude in the postmaneuver orbit at distance r_T from the center of attraction. Substitution of the expression for v_T^2 from Equation (14) into Equation (15) yields, after some algebraic manipulation, the equation

$$\frac{(\dot{X}^2 + \dot{Y}^2)[1 - r_o^2/(r_T \sin \beta_T)^2]}{(2\mu/r_o)(1 - r_o/r_T)} + \frac{\dot{Z}^2}{(2\mu/r_o)(1 - r_o/r_T)} = 1 \quad . \tag{16}$$

If $r_T < r_o$, then Equation (16) defines a hyperboloid of one sheet whose intersection with the X-Z plane is shown in Figure 4. If $r_T > r_o$, then the geometric figure represented by Equation (16) depends on $\sin \beta_T$. When $\sin \beta_T < (r_o/r_T)$ the figure is a hyperboloid of two sheets that degenerates into two parallel planes at $\sin \beta_T = (r_o/r_T)$. When $\sin \beta_T > (r_o/r_T)$, the figure is an ellipsoid. The intersections of the constraint surfaces with the X-Z plane for these latter three cases in shown in Figure 5. In all cases, the surfaces are symmetrical about the origin and about the Z-axis. The applicable surface in three-dimensional velocity space for each case can be visualized as that which is swept out by the appropriate curve in Figure 4 or Figure 5, as it is rotated about the Z-axis.

Now consider the special case where r_T represents the desired distance of one of the apsides (either perigee or apogee) from the center of attraction. If the subscript α is used to designate apsidal conditions in lieu of the general subscript T, then r_T is replaced by r_α, $\cos \beta_T$ is replaced by 0, and $\sin \beta_T$ is replaced by 1 in the preceding equations, since the flight

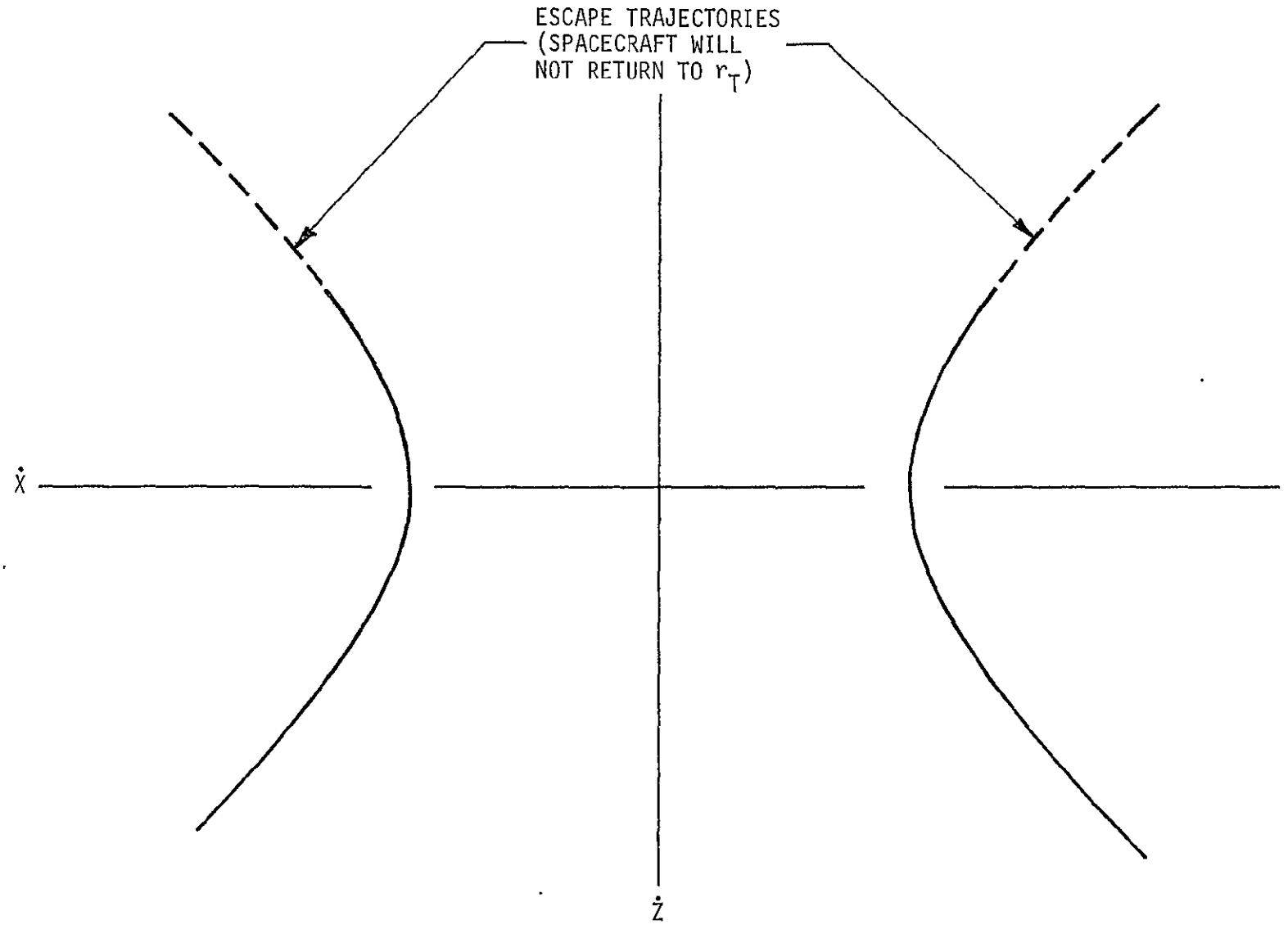

Figure 4. Intersection of r_T, β_T Constraint Surface with X-Z Plane ($r_T < r_o$)

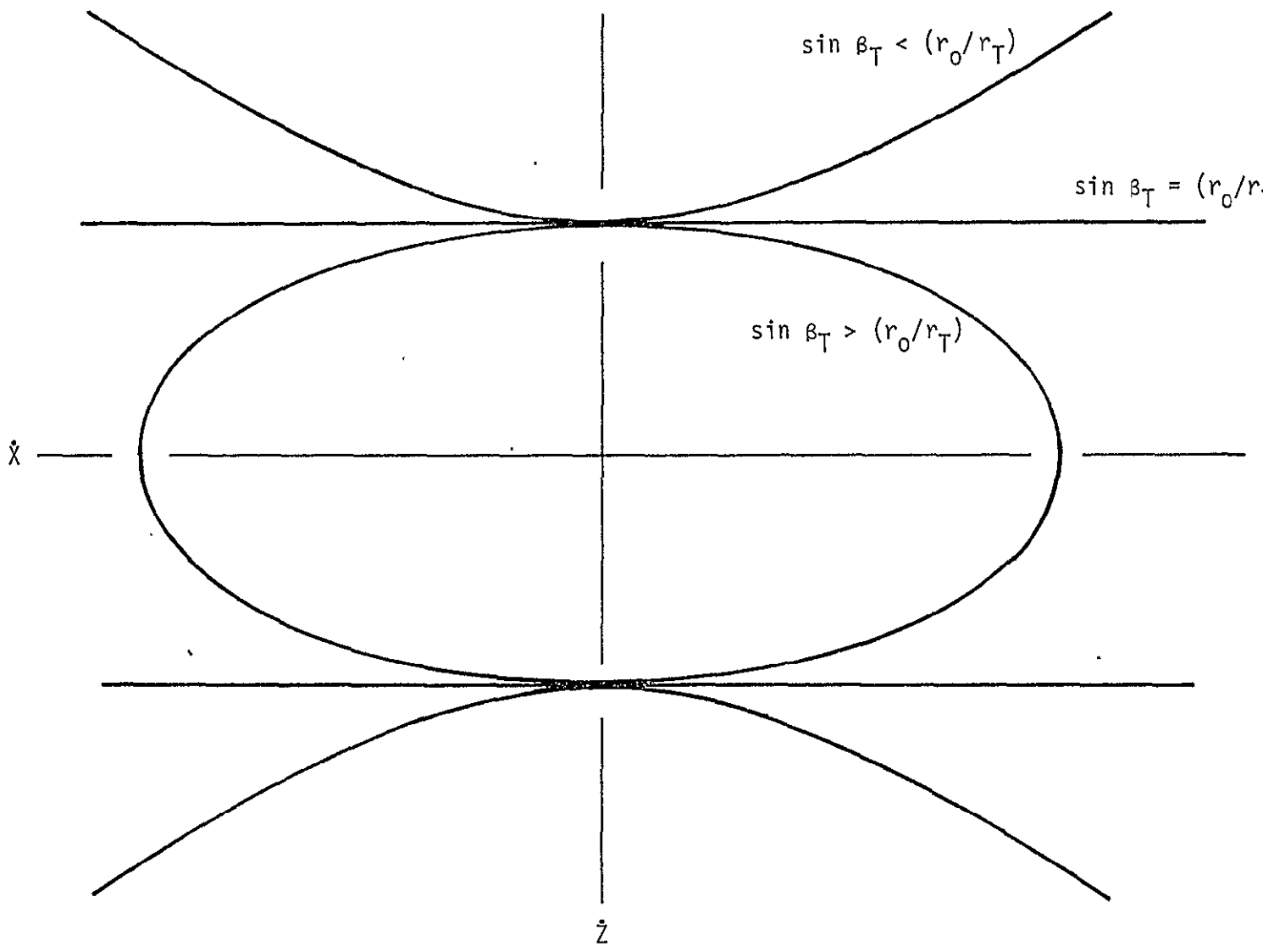

Figure 5. Intersection of r_T, β_T Constraint Surfaces with X-Z Plane ($r_T > r_o$)

path angle β must be equal to 90 degrees at either apsis. Again, taking up first the trivial case where $r_\alpha = r_o$, Equation (13) becomes

$$\dot{Z}^2 = 0 \quad , \tag{17}$$

which is of course the equation of a horizontal plane in velocity space. For the non-trivial case (where $r_\alpha \neq r_o$), Equation (16) can be simplified to the form

$$\frac{(\dot{X}^2 + \dot{Y}^2)(1 + r_o/r_\alpha)}{(2\mu/r_o)} + \frac{\dot{Z}^2}{(2\mu/r_o)(1 - r_o/r_\alpha)} = 1 \quad . \tag{18}$$

Note that the first term in Equation (18) is always postive, and that the second term is positive or negative depending on whether r_α is greater than or less than r_o. Physically, of course, if r_α is greater than r_o it must represent the apogee distance r_A, and if it is less than r_o it must represent the perigee distance r_P. For the general case where $r_P < r_o < r_A$, the two equations

$$\frac{(\dot{X}^2 + \dot{Y}^2)(1 + r_o/r_A)}{(2\mu/r_o)} + \frac{\dot{Z}^2}{(2\mu/r_o)(1 - r_o/r_A)} = 1 \tag{19}$$

and

$$\frac{(\dot{X}^2 + \dot{Y}^2)(r_o/r_P + 1)}{(2\mu/r_o)} - \frac{\dot{Z}^2}{(2\mu/r_o)(r_o/r_P - 1)} = 1 \quad , \tag{20}$$

must be satisfied simultaneously. Equations (19) and (20), respectively, define an ellipsoid and a hyperboloid of one sheet whose intersections with the X - Z plane are illustrated in Figure 6. The intersections of the ellipsoid and hyperboloid with each other form two parallel circles in velocity space whose equations are

$$\dot{Z}_\ell = \pm \sqrt{\left(\frac{2\mu}{r_o}\right) \frac{(1 - r_o/r_A)(r_o/r_P - 1)}{(r_o/r_P + r_o/r_A)}} \tag{21}$$

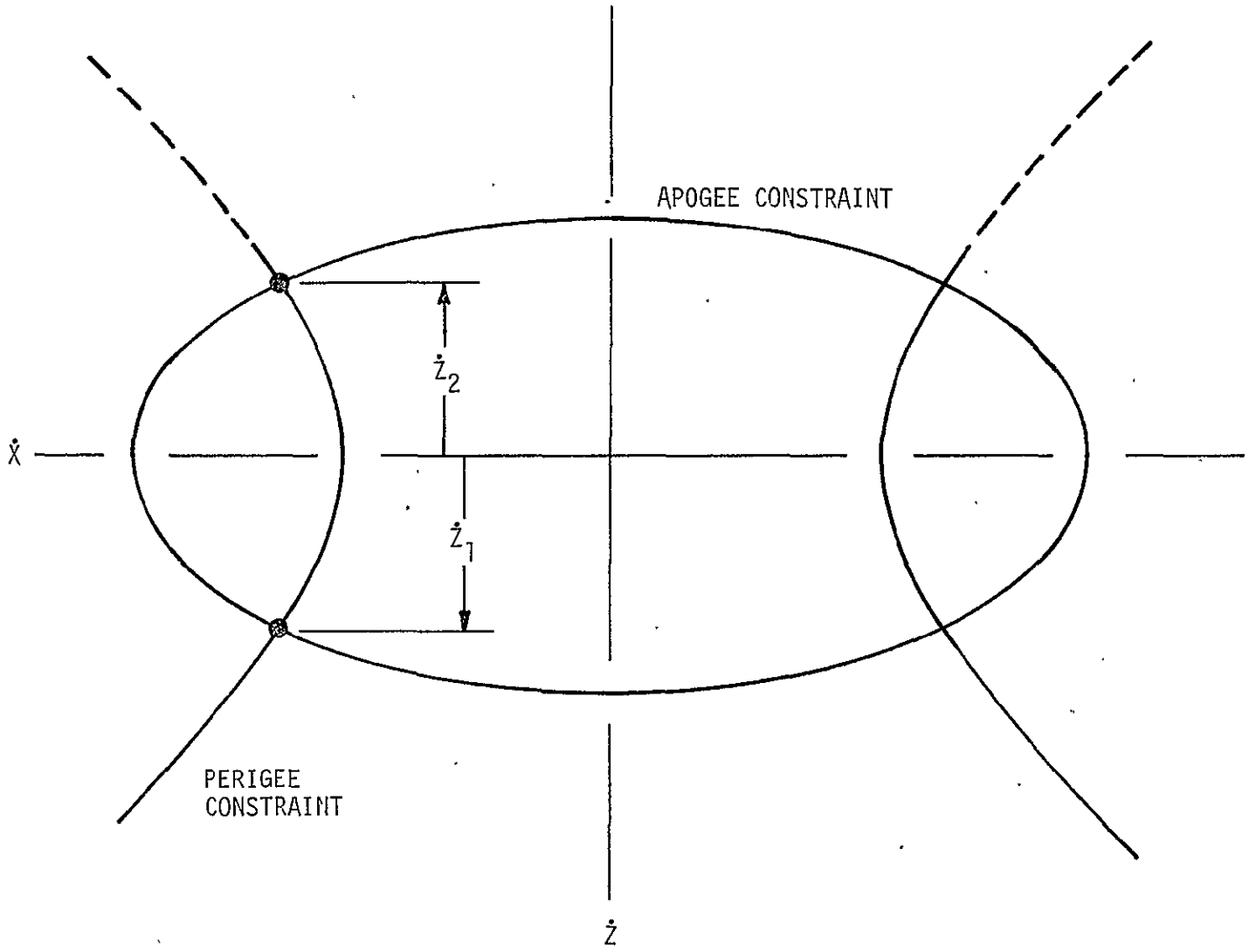

Figure 6. Intersection of Apogee and Perigee Constraint Surfaces with X-Z Plane ($r_p < r_o < r_A$)

and

$$\dot{X}^2 + \dot{Y}^2 = \frac{(2\mu/r_o)}{(r_o/r_P + r_o/r_A)} \quad , \tag{22}$$

and where the subscript ℓ is assigned a value of 1 when the minus sign is used and a value of 2 when the plus sign is used. The two circles can be visualized as those which are swept out by the points of intersection between the ellipse and one branch of the hyperbola shown in Figure 6, as they are rotated about the Z-axis.

Given r_o, r_A, and r_P, Equation (21) can be used to compute the two numerical values of $\dot{Z}$ that will satisfy the targeting constraints. These values can be substituted into Equation (5), along with the expression

$$\dot{Y}^2 = \frac{(2\mu/r_o)}{(r_o/r_P + r_o/r_A)} - \dot{X}^2 \tag{23}$$

from Equation (22), to obtain two linear equations in $\dot{X}$ of the form

$$\dot{X}_\ell = \frac{\dot{X}_o^2 + (\dot{Z}_\ell - \dot{Z}_o)^2 + (2\mu/r_o)/(r_o/r_P + r_o/r_A) - V^2}{2\,\dot{X}_o} \quad , \tag{24}$$

where ℓ takes on the values 1 and 2. Finally, the targeting solution is completed by substituting the numerical values of $\dot{X}_1$ and $\dot{X}_2$ back into Equation (23), obtaining

$$\dot{Y}_{\ell,m} = \pm\sqrt{\frac{(2\mu/r_o)}{(r_o/r_P + r_o/r_A)} - \dot{X}_\ell^2} \quad . \tag{25}$$

Again, the subscript ℓ takes on the values 1 and 2, and for each value of ℓ the subscript m is assigned a value of 1 when the minus sign is used in Equation (25), and a value of 2 when the plus sign is used. Of course, only real values of $\dot{Y}_{\ell,m}$ are acceptable.

If the radicand in Equation (25) is positive for both values of ℓ, then there are four physical solutions of the maneuver targeting problem. As in the case of the orbit circularization problem, the values of $\dot{Y}_{\ell,m}$ will not be zero in general, which means that an orbital plane change generally will be necessary if specific values of apogee and perigee altitude are to be attained with a single velocity increment of fixed magnitude.

3.1.3 Achievement of Specified Orbit Period and Apsis Altitude

Requiring the postmaneuver orbit to have a specified period P defines a sphere in velocity space whose equation is

$$\dot{X}^2 + \dot{Y}^2 + \dot{Z}^2 = (2\mu/r_o) - (2\pi\mu/P)^{2/3} \quad . \tag{26}^*$$

If it is desired also to achieve a specified apsidal distance r_α, then Equations (18) and (26) must be satisfied simultaneously. The loci of solutions (if any exist) are two parallel circles whose equations are

$$\dot{Z}_\ell = \pm\sqrt{\left(\frac{2\mu}{r_o}\right)\frac{(r_o/r_\alpha - 1)}{(r_o/r_\alpha)} - \left(\frac{2\pi\mu}{P}\right)^{2/3}\left[\frac{(r_o/r_\alpha)^2 - 1}{(r_o/r_\alpha)^2}\right]} \tag{27}$$

and

$$\dot{X}^2 + \dot{Y}^2 = \frac{(r_o/r_\alpha)(2\mu/r_o) - (2\pi\mu/P)^{2/3}}{(r_o/r_\alpha)^2} \quad , \tag{28}$$

where the subscript ℓ is assigned a value of 1 when the minus sign is used and a value of 2 when the plus sign is used.

Given r_o, r_α, and P, Equation (27) can be used to compute the two numerical values of $\dot{Z}$ that will satisfy the targeting constraints. These values can be substituted into Equation (5), along with the expression

$$\dot{Y}^2 = \frac{(r_o/r_\alpha)(2\mu/r_o) - (2\pi\mu/P)^{2/3}}{(r_o/r_\alpha)^2} - \dot{X}^2 \tag{29}$$

*If $(2\mu/r_o) - (2\pi\mu/P)^{2/3} < 0$, of course there is no physical solution to the problem.

from the Equation (28) to obtain two linear equations in $\dot{X}$ of the form

$$\dot{X}_\ell = \frac{\dot{X}_o^2 + (\dot{Z}_\ell - \dot{Z}_o)^2 + \left[(r_o/r_\alpha)(2\mu/r_o) - (2\pi\mu/P)^{2/3} \right] / (r_o/r_\alpha)^2 - V^2}{2\,\dot{X}_o} \quad (30)$$

where ℓ takes on the values 1 and 2. The targeting solution is completed by substituting the numerical values of $\dot{X}_1$ and $\dot{X}_2$ back into Equation (29) to obtain

$$\dot{Y}_{\ell,m} = \pm\sqrt{\frac{(r_o/r_\alpha)(2\mu/r_o) - (2\pi\mu/P)^{2/3}}{(r_o/r_\alpha)^2} - \dot{X}_\ell^2} \quad . \quad (31)$$

As before, the subscript ℓ takes on the values 1 and 2, and for each value of ℓ the subscript m is assigned a value of 1 when the minus sign is used in Equation (31) and a value of 2 when the plus sign is used. And again, of course, only real values of $\dot{Y}_{\ell,m}$ represent acceptable solutions.

3.1.4 Achievement of Specified Orbit Period and Wedge Angle

Imposing an equality constraint on the wedge angle W (the angle through which the orbit plane is rotated by the velocity impulse) defines a half-plane in velocity space whose equation is

$$\dot{X} \sin W = \dot{Y} \cos W \quad , \quad (32)$$

where $\dot{X}$ is required to have the sign of cos W and $\dot{Y}$ is required to have the sign of sin W. The intersection of this half-plane with the sphere defined by Equation (26) is a semicircle whose radius is equal to

$$\sqrt{(2\mu/r_o) - (2\pi\mu/P)^{2/3}} \quad .$$

First consider the case where cos W = 0. Equation (32) then yields

$$\dot{X}^2 = 0 \quad , \quad (33)$$

which can be substituted into Equations (5) and (26) to obtain

$$\dot{Y}^2 + (\dot{Z} - \dot{Z}_o)^2 = V^2 - \dot{X}_o^2 \tag{34}$$

and

$$\dot{Y}^2 + \dot{Z}^2 = (2\mu/r_o) - (2\pi\mu/P)^{2/3} \quad , \tag{35}$$

where of course the right hand sides of both equations must be greater than or equal to zero if a real solution is to exist. Expanding Equation (34) and then subtracting it from Equation (35) yields the linear equation

$$\dot{Z} = \frac{\dot{X}_o^2 + \dot{Z}_o^2 - V^2 + (2\mu/r_o) - (2\pi\mu/P)^{2/3}}{2\,\dot{Z}_o} \tag{36}^*$$

which can be used to obtain a numerical value of $\dot{Z}$. This numerical value can be used in the equation

$$\dot{Y} = \sqrt{V^2 - \dot{X}_o^2 - (\dot{Z} - \dot{Z}_o)^2}\ \sin W \tag{37}$$

to complete the solution for the special case of cos W = 0. Equation (37) is derived from Equation (34) and the condition imposed on Equation (32) regarding the sign of $\dot{Y}$.

Now consider the case where cos $W \neq 0$. Equation (32) yields

$$\dot{Y} = \dot{X} \tan W \quad , \tag{38}$$

which can be substituted into Equations (5) and (26) to obtain

$$(\dot{X} - \dot{X}_o)^2 + \dot{X}^2 \tan^2 W + (\dot{Z} - \dot{Z}_o)^2 = V^2 \tag{39}$$

---

*If $\dot{Z}_o = 0$, then a solution is possible only if $\dot{X}_o^2 + \dot{Z}_o^2 - V^2 + (2\mu/r_o) - (2\pi\mu/P)^{2/3} = 0$.

and

$$\dot{X}^2 + \dot{X}^2 \tan^2 W + \dot{Z}^2 = (2\mu/r_o) - (2\pi\mu/P)^{2/3} \quad . \tag{40}$$

Expanding Equation (39) and subtracting it from Equation (40) yields

$$Q_1 - \dot{X}_o \dot{X} = \dot{Z}_o \dot{Z} \quad , \tag{41}$$

where

$$2Q_1 = (2\mu/r_o) - (2\pi\mu/P)^{2/3} - V^2 + \dot{X}_o^2 + \dot{Z}_o^2 \quad . \tag{42}$$

If $\dot{Z}_o = 0$, then Equation (41) can be used to obtain a numerical value for $\dot{X}$, thus

$$\dot{X} = Q_1/\dot{X}_o \quad . \tag{43}$$

If the computed value of $\dot{X}$ does not have the same sign as cos W, then there is no solution to the problem. If the numerical value of $\dot{X}$ does have the same sign as cos W, then it can be substituted into Equation (38) to obtain $\dot{Y}$. In this case, the two permissable values of $\dot{Z}$ are found by substituting the numerical value of $\dot{X}$ into Equation (40), yielding

$$\dot{Z}_\ell = \pm\sqrt{(2\mu/r_o) - (2\pi\mu/P)^{2/3} - (\dot{X}/\cos W)^2} \quad , \tag{44}$$

where ℓ is assigned the value 1 when the minus sign is used in Equation (44) and the value 2 when the plus sign is used.

If $\dot{Z}_o \neq o$, then the solution is found by squaring both sides of Equation (41) and substituting an expression for Z^2 from Equation (40) into the result, thus:

$$Q_1^2 - 2Q_1 \dot{X}_o \dot{X} + \dot{X}_o^2 \dot{X}^2 = \dot{Z}_o^2 \left[(2\mu/r_o) - (2\pi\mu/P)^{2/3} - \dot{X}^2 (1 + \tan^2 W) \right] \quad . \tag{45}$$

Equation (45) can be arranged in the quadratic form

$$A_1 \dot{X}^2 + A_2 \dot{X} + A_3 = 0 \quad , \tag{46}$$

which has the roots

$$\dot{X}_\ell = \left(- A_2 \pm \sqrt{A_2^2 - 4A_1 A_3} \right) / 2A_1 \quad , \tag{47}$$

where

$$A_1 = \dot{X}_o^2 + (\dot{Z}_o / \cos W)^2 \quad , \tag{48}$$

$$A_2 = - 2Q_1 \dot{X}_o \quad , \tag{49}$$

and

$$A_3 = Q_1^2 - \dot{Z}_o^2 \left[(2\mu / r_o) - (2\pi\mu / P)^{2/3} \right] \quad , \tag{50}$$

and where ℓ is assigned the value 1 when the minus sign is used in Equation (47) and the value 2 when the plus sign is used. Only those real values of $\dot{X}_\ell$ that have the same sign as cos W satisfy the wedge angle constraint. The acceptable values of $\dot{X}_\ell$ (if any) can be substituted into Equations (38) and (41) to obtain the associated values of $\dot{Y}$ and $\dot{Z}$.

3.1.5 Achievement of Specified Apsis Altitude and Wedge Angle

This targeting problem requires the simultaneous satisfaction of Equations (5), (18), and (32). The conditions associated with Equation (32) regarding the sign of $\dot{X}$ and of $\dot{Y}$, as delineated in Section 3.1.4, must also be satisfied.

Again, consider first the case where cos W = 0. Substitution of $\dot{X}^2 = 0$ from Equation (33) into Equation (18) yields

$$\dot{Y}^2 \left[1 - (r_o / r_\alpha)^2 \right] + \dot{Z}^2 = (2\mu / r_o)(1 - r_o / r_\alpha) \quad . \tag{51}$$

Equation (34), which resulted from substituting $\dot{X}^2 = 0$ into Equation (5), can be subtracted from Equation (51) to obtain

$$2\dot{Z}_o \dot{Z} = (r_o/r_\alpha)^2 \dot{Y}^2 - 2Q_2 \quad , \tag{52}$$

where

$$2Q_2 = V^2 - \left(\dot{X}_o^2 + \dot{Z}_o^2 \right) - (2\mu/r_o)(1 - r_o/r_\alpha) \quad . \tag{53}$$

If $\dot{Z}_o = 0$, Equation (52) and the sign conditions associated with Equation (32) yield immediately

$$\dot{Y} = \left[\sqrt{2Q_2} \,/\, (r_o/r_\alpha) \right] \sin W \quad . \tag{54}$$

There is no solution to the problem if $Q_2 \leq 0$. Assuming $Q_2 > 0$, the numerical value obtained from Equation (54) can be substituted into Equation (51) to solve for $\dot{Z}$, thus:

$$\dot{Z}_\ell = \pm\sqrt{(1 - r_o/r_\alpha) \left[(2\mu/r_o) - (1 + r_o/r_\alpha) \dot{Y}^2 \right]} \tag{55}$$

where ℓ is assigned a value of 1 when the minus sign is used and a value of 2 when the plus sign is used.

If $\dot{Z}_o \neq 0$, the solution is obtained by squaring both sides of Equation (52). Then an expression for $\dot{Z}^2$, obtained from Equation (51), can be substituted into the result to produce

$$B_1 \dot{Y}^4 + B_2 \dot{Y}^2 + B_3 = 0 \tag{56}$$

which has the roots

$$\dot{Y}_\ell^2 = \left(- B_2 \pm \sqrt{B_2^2 - 4B_1 B_3} \right) / 2B_1 \tag{57}$$

where

$$B_1 = (r_0/r_\alpha)^4/4 \quad , \tag{58}$$

$$B_2 = \dot{Z}_0^2 \left[1 - (r_0/r_\alpha)^2 \right] - (r_0/r_\alpha)^2 Q_2 \quad , \tag{59}$$

and

$$B_3 = Q_2^2 - \dot{Z}_0^2 (2\mu/r_0)(1 - r_0/r_\alpha) \quad , \tag{60}$$

and where ℓ is assigned the value 1 when the minus sign is used in Equation (57) and the value 2 when the plus sign is used. For each of the real positive values of $\dot{Y}_\ell^2$ (if any) obtained from Equation (57), the out-of-plane postmaneuver velocity component is given by

$$\dot{Y}_\ell = \sqrt{\dot{Y}_\ell^2} \sin W \quad . \tag{61}$$

The radial velocity components are found by substituting the computed values of $\dot{Y}_\ell$ into Equation (52).

Now, consider the case where $\cos W \neq 0$. Subsititution of Equation (38) into Equation (18) yields

$$\frac{\dot{X}^2 (1 + \tan^2 W)(1 + r_0/r_\alpha)}{(2\mu/r_0)} + \frac{\dot{Z}^2}{(2\mu/r_0)(1 - r_0/r_\alpha)} = 1 \quad , \tag{62}$$

from which Equation (39) can be subtracted to obtain

$$\dot{Z}_0 \dot{Z} = Q_3 \dot{X}^2 - \dot{X}_0 \dot{X} - Q_2 \quad , \tag{63}$$

where

$$2Q_3 = (r_0/r_\alpha)^2 (1 + \tan^2 W) \tag{64}$$

and where Q_2 is given by Equation (53).

If $\dot{Z}_o = 0$, then Equation (63) reduces to

$$Q_3 \dot{X}^2 - \dot{X}_o \dot{X} - Q_2 = 0 \qquad (65)$$

which has the roots

$$\dot{X}_\ell = \left(\dot{X}_o \pm \sqrt{\dot{X}_o^2 + 4Q_2 Q_3} \right) / (2Q_3) \quad , \qquad (66)$$

where ℓ is assigned the value 1 or 2 depending on whether the minus sign or the plus sign is used in Equation (66). Only those roots of Equation (65) that are real and that have the same sign as cos W are acceptable. For the acceptable values of $\dot{X}_\ell$, the corresponding values of $\dot{Y}_\ell$ are obtained from Equation (38). The postmaneuver radial velocity components are obtained from Equation (62), thus:

$$\dot{Z}_{\ell,m} = \pm \sqrt{(2\mu/r_o)(1 - r_o/r_\alpha) - \left[1 - (r_o/r_\alpha)^2 \right] (\dot{X}_\ell/\cos W)^2} \qquad (67)$$

where, for each of the two possible values of ℓ, the subscript m is assigned a value of 1 or 2 depending on whether the minus sign or the plus sign is used in Equation (67).

If $\dot{Z}_o \neq 0$, both sides of Equation (63) are squared and an expression for $\dot{Z}^2$ is obtained from Equation (62) and substituted into the result. This yields

$$C_1 \dot{X}^4 + C_2 \dot{X}^3 + C_3 \dot{X}^2 + C_4 \dot{X} + C_5 = 0 \quad , \qquad (65)$$

where

$$C_1 = Q_3^2 \quad , \qquad (66)$$

$$C_2 = -2Q_3 \dot{X}_o \quad , \qquad (67)$$

$$C_3 = \dot{X}_o^2 - 2Q_2 Q_3 + (\dot{Z}_o/\cos W)^2 \left[1 - (r_o/r_\alpha)^2 \right] \quad , \qquad (68)$$

$$C_4 = 2Q_2 \dot{X}_o \quad , \qquad (69)$$

and

$$C_5 = Q_2^2 - \dot{Z}_o^2 (2\mu/r_o)(1 - r_o/r_\alpha) \quad . \tag{70}$$

The numerical values $\dot{X}_\ell$ (where $\ell = 1, 2, 3, 4$) which satisfy Equation (65) can be computed by using an explicit algorithm which exists for finding the roots of a quartic equation. Of the four possible roots, only those which are real and which have the same sign as cos W are acceptable. Given any acceptable value $\dot{X}_\ell$, the corresponding value $\dot{Y}_\ell$ can be obtained from Equation (38) and $\dot{Z}_\ell$ can be obtained from Equation (63).

3.2 TWO-IMPULSE ORBITAL TRANSFER WITHOUT PHASING CONSTPAINT

The orbit of any satellite can be defined completely by six scalar orbit constants, such as the following classical set*:

p	semilatus rectum
e	eccentricity
i	inclination
Ω	right ascension of the ascending node
ω	argument of perigee
t_p	time of perigee passage.

That is to say, given appropriate numerical values for these six scalars, the position and velocity of the satellite can be calculated at any arbitrary time t.

The first five quantities listed in the preceding paragraph define the size and shape of the orbit and its orientation in an equatorial inertial reference frame. They provide sufficient information to calculate satellite position and velocity vectors as functions of a geometric variable such as the true anomaly f. The sixth quantity (t_p) is a phasing constant whose value must be known to calculate the satellite position and velocity as a function of time.

*This set is completely definitive for all orbits except those involving rectilinear motion, where p = 0 and e = 1 and consequently the orbital energy cannot be calculated. In such a case (which is not considered to be of interest here), the value of some other parameter such as the semimajor axis a must be known.

The problem to be considered in this section is that of transferring a spacecraft from a fully defined initial orbit to a target orbit whose size, shape, and orientation (p, e, i, Ω, ω) are given as input but whose phasing constant (t_p) is not specified. Furthermore, the transfer is to be effected by two velocity increments, at least one of which is required to have a specific magnitude.

If the positions of both impulse points and the orientation of the transfer orbit angular momentum vector are known, then there exists a "singly-constrained" analytic solution to determine explicitly just which transfer trajectories (if any) will satisfy a ΔV constraint at one end or the other of the transfer arc. Often it will be necessary to satisfy arbitrary constraints on velocity increment magnitude at <u>both</u> ends of the transfer arc. No explicit solution is known for the latter problem. However, doubly-constrained solutions can be found by a straightforward procedure which involves "scanning" singly-constrained solution families. The scanning is accomplished by systematically varying the values of two independent variables that jointly define the two impulse locations and the direction of the transfer orbit angular momentum vector. Depending on the overall nature of the trajectory design problem, it may be preferable when generating the singly-constrained analytic solutions to satisfy the ΔV constraint on either the final or the initial impulse. Assume for the sake of argument that it is chosen to satisfy the constraint on the initial impluse. Then it is a simple matter, each time a singly-constrained solution is found, to calculate the required final ΔV as an output variable. Since every member of the solution family satisfies the ΔV constraint on the initial impulse, the solutions to the doubly-constrained problem can be found (if they exist) by examining the output data to determine which combinations of independent variable values produce the desired final ΔV.

Of course there are many other transfer trajectory parameters besides the magnitude of the unconstrained velocity increment which can be computed as output from the singly-constrained solution, and which may have to be considered in the selection of a transfer trajectory. Given an array of data resulting from a systematic scan of two independent variables, general-purpose software is available for generating a display which depicts the

behavior of any selected set of output variables over the entire two-dimensional scan space (Reference 4, pp. 12-13). The ability to utilize such a capability to solve this type of trajectory design problem is highly desirable. The key to successful utilization lies in the identification of a pair of scalar independent variables $\overline{X}$ and $\overline{Y}$ such that a systematic variation of their values will generate all possible solutions of interest.

3.2.1 Selection of Scan-Control Variables

In general, the planes of the initial orbit and the target orbit will be inclined to one another at some angle Δ. As illustrated in Figure 7, the position of the initial impulse can be defined by the angle λ_I, which is measured from a relative node (say, the ascending node of the initial orbit on the target orbit plane) in the direction of orbital motion in the initial orbit. The position of the final impulse can be defined by the angle λ_T, measured from the same relative node in the direction of motion in the target orbit plane. The transfer angle θ is measured from the initial impulse point to the final impulse point, in the direction of motion in the transfer orbit. The transfer orbit makes the wedge angles W_I and W_T, respectively, with the initial orbit plane and the target orbit plane. The wedge angles are measured from the appropriate (initial or target) orbit plane to the transfer orbit plane, and are positive in the direction of clockwise rotation when viewed from a vantage point above the appropriate impulse point, looking downward toward the center of gravitational attraction.

The positions of the impulse points obviously can be defined by specifying values for λ_I and λ_T. However, this combination of variables would not be a good choice as the only method of scan control because their systematic variation would not generate the solution families which are associated with nodal transfer (i.e., where $\lambda_I = 0°$ and $\lambda_T = 180°$ or $\lambda_I = 180°$ and $\lambda_T = 360°$). In a nodal transfer case the number of possible transfer orbit planes is infinite. Consequently it is necessary to specify the value of some additional input quantity, such as the wedge angle at one of the impulse points, in order to generate a unique solution.

There is no ambiguity at any point regarding the orientation of the transfer orbit plane if, say, λ_I and W_I are chosen as scan control variables.

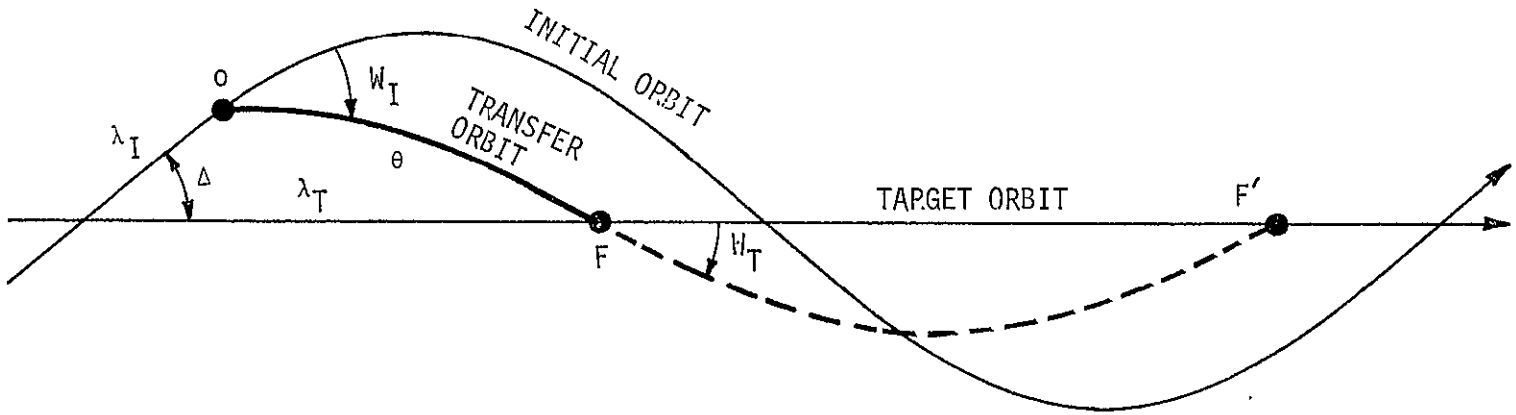

Figure 7. Geometry of Orbital Transfer Problem

Again, this would not be a good choice as the only method of scan control because (for instance) when $\lambda_I = 0$ and $W_I = \Delta$, the number of possible locations for the second impulse is infinite and some other input quantity such as λ_T must be input to generate a unique solution.

It turns out, unfortunately, that there is no single pair of independent variables whose systematic variation will generate all of the solutions which might be of interest in this type of trajectory design problem. However, all possible solutions can be generated by separately scanning at most two sets of independent variables, such as those designated as Set No. 1, 2, 3, and 4 in Table 1. As indicated in the table, Sets 1 and 2 apply when the singly-constrained analytic solution is to satisfy an equality constraint on the magnitude of the initial impulse, and Sets 3 and 4 apply when an equality constraint is to be applied to the final impulse magnitude in the analytic solution.

For any one set of independent variables, there are certain combinations of values which will produce "manifold ambiguties" (i.e., situations in which there are infinite number of possible solutions) of the type previously discussed, wherein a whole family of solutions is obscured by the particular choice of independent variables. The conditions which characterize these situations are shown in Table 1, along with suggested "resolutions" (i.e., arbitrary conditions to be imposed for the purpose of generating one unique solution from the obscured family). The true resolution of any manifold ambiguity requires a separate scan of the appropriate alternative variable set, which allows the obscured family to be surveyed in its entirety.

In addition to the manifold ambiguities associated with particular combinations of independent variable values, there is a "twofold ambiguity" associated with every combination of values. In the cases where λ_I and λ_T are specified, this arises from the possibility of two opposite orientations of the transfer orbit angular momentum vector. The suggested resolution in such cases is to require the cosine of the wedge angle at the constrained impulse point to have a particular sign, as defined by an auxiliary input variable H that is required to have the value + 1.0 or - 1.0 throughout any particular scanning operation. In the cases where λ_I and W_I or where λ_T and W_T are specified, the twofold ambiguity arises from the fact that

Table 1. Scan Control Data

INDEPENDENT VARIABLE SET NO. (ISET)	IMPULSE AT WHICH ΔV CONSTRAINT IS APPLIED	DEFINITION OF SCAN CONTROL VARIABLES		RESOLUTION OF TWOFOLD AMBIGUITY	MANIFOLD AMBIGUITY	
		$\overline{X}$	$\overline{Y}$		CONDITION FOR OCCURRENCE	RESOLUTION
1	INITIAL	λ_I	W_I	$\cos\theta = H\sqrt{1 - \sin^2\theta}$	$\sin W_T = 0$	$\sin^2\theta = 0$
2	INITIAL	λ_I	λ_T	$\cos W_I = -H\sqrt{1 - \sin^2 W_I}$	$\sin\theta = 0$	$\sin^2 W_I = \sin^2\Delta$
3	FINAL	λ_T	W_T	$\cos\theta = H\sqrt{1 - \sin^2\theta}$	$\sin W_I = 0$	$\sin^2\theta = 0$
4	FINAL	λ_T	λ_I	$\cos W_T = -H\sqrt{1 - \sin^2 W_T}$	$\sin\theta = 0$	$\sin^2 W_T = \sin^2\Delta$

the transfer angle θ may have either of two values which differ by 180°. The suggested resolution in such cases is to have the aforementioned variable H define the sign of cos θ.

The equations shown in Table 1 for the resolution of twofold ambiguities are designed such that, in each case, the subset of transfer orbits associated with a value of H = - 1.0 will generally require lower ΔV magnitudes than the subset associated with a value of H = + 1.0. This increases the probability that all possible solutions for a particular problem can be generated by using only one of the two allowable values of H.

3.2.2 Selection of Reference Node

In the general case where sin $\Delta >> 0$, it makes little difference which of the relative modes between the initial and target orbit planes is used as a reference for measuring λ_I and λ_T. Either the ascending or the descending node of one orbit on the plane of the other might be chosen, so long as it is used consistently. However, when sin $\Delta << 1$ (i.e., when the orbits are nearly coplanar), special considerations may have to be taken into account if discontinuities are to be avoided in the output data between separate scans over neighboring orbits, or between successive discrete solutions in an iterative precision targeting process.

When the initial orbit and the target orbit are coplanar, the relative node line is of course undefined. The orbits can be coplanar only if $i_I = i_T$ or if $i_I = 180° - i_T$. In all cases but the very special one where sin i_I = sin i_T = 0, it is also necessary that $\Omega_I = \Omega_T$ when $i_I = i_T$ or that $\Omega_I = \Omega_T \pm 180°$ when $i_I = 180° - i_T$. Because gravitational harmonics generally produce different values for the nodal regression rates $\dot{\Omega}_I$ and $\dot{\Omega}_T$, perfect coplanarity between satellite orbits is at most a fleeting circumstance in the real world of orbital flight operations.

Figure 8 illustrates a typical case of the type under consideration where, for simplicity, the plane of the target orbit is assumed to be stationary. If perfect coplanarity occurs at the time t^*, then between the times $t^* - \varepsilon$ and $t^* + \varepsilon$ there is a discontinuous change of 180° in the inertial

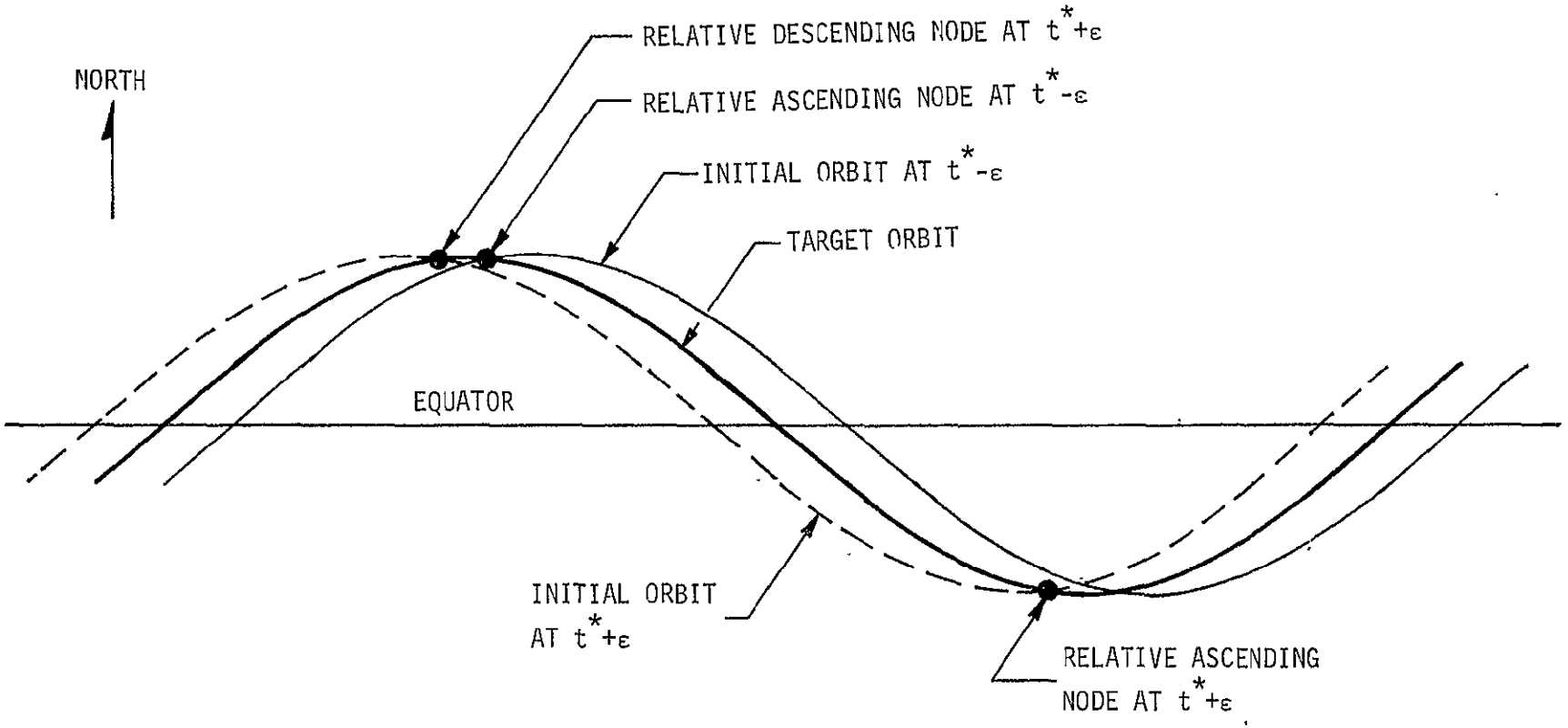

Figure 8. Node Shift Geometry for Nearly Coplanar Orbits

locations of both the ascending and the descending relative nodes. If either of these nodes were used as the reference for measuring λ_I and λ_T, then clearly there would also be, within the same time interval, discontinuous changes of 180° in the inertial directions of impulse position vectors defined by fixed values of λ_I and λ_T.

It can be seen by inspecting Figure 8 that the northerly and southerly (as distinguished from the ascending and descending) relative nodes approach the positions defined by $u = 90°$ and $u = 270°$, respectively, as ε (hence also $\sin \Delta$) approaches zero, where u is the argument of latitude in either the initial or the target orbit. It follows that the discontinuities just described can be removed if λ_I and λ_T are referenced to, say, the northerly relative node when $\sin \Delta \neq 0$ and to the position defined by $u = 90°$ when $\sin \Delta = 0$.

Although the convention described in the preceding paragraph is to be preferred when the initial and final orbits are in the neighborhood of coplanarity, unfortunately it can not be used generally for all orbit combinations. To do so could produce discontinuities, similar to those previously described, whenever the relative nodes happen to lie in the vicinity of the equator. Since the choice of convention is necessary to avoid discontinuities between rather than within separate scans or discrete solutions, there is no basis for making such a choice within the logic of the analytic solution itself. Therefore it is necessary to provide an input flag IREF which can be given either of two values by the trajectory analyst, specifying whether the reference for measuring λ_I and λ_T is to be the northerly relative node or the ascending relative node.

3.2.3 Calculation of Position and Velocity Vectors in the Initial and the Target Orbits

The purpose in this section is to define equations for calculating position and velocity vectors in the initial and the target orbits as functions of the independent variable set identification flag ISET and the associated scan control variables $\underline{X}$ and $\underline{Y}$ which are defined in Table 1, the auxiliary input variable H, and the reference convention flag IREF. These computations are necessary to generate inputs to the transfer orbit velocity vector equations which will be defined in Section 3.2.4. Only the case where

the ΔV constraint is to be applied to the initial impulse (ISET = 1 or 2) will be addressed specifically. The logic and equations for the other case (ISET = 3 or 4) can be obtained by replacing ISET with ISET + 2, changing the sign of the transfer angle θ, and interchanging the subscripts I and T or the words "initial" and "target" wherever they appear in the following discussion.

To facilitate subsequent computations, it is convenient to define the geocentric inertial components of a set of unit vectors relating to the initial and target orbits. In general for any orbit the unit vector pointing in the direction of its ascending node on the equator is given by

$$\hat{\Omega} = \begin{bmatrix} \cos \Omega \\ \sin \Omega \\ 0 \end{bmatrix} . \tag{74}$$

The unit vector

$$\hat{J} = \begin{bmatrix} - \sin \Omega \sin i \\ \cos \Omega \sin i \\ - \cos i \end{bmatrix} \tag{75}$$

points in a direction opposite to that of the angular momentum, and the unit vector

$$\hat{U} = \hat{\Omega} \times \hat{J} \tag{76}$$

is directed toward the point of maximum northerly declination in the orbit. The unit vectors

$$\hat{K} = - \hat{\Omega} \cos \omega - \hat{U} \sin \omega \tag{77}$$

and

$$\hat{I} = \hat{J} \times \hat{K} \tag{78}$$

complete an orthogonal triad ($\hat{I}$, $\hat{J}$, $\hat{K}$) which defines the local vertical coordinate system <u>at perigee</u> just as the triad ($\hat{i}$, $\hat{j}$, $\hat{k}$) used in Section 3.1 defines the local vertical coordinate system at an arbitrary point in the orbit.

The cosine of the relative inclination between the two orbits is given by

$$\cos \Delta = \hat{J}_T \cdot \hat{J}_I \tag{79}$$

and the sine by

$$\sin \Delta = \sqrt{1 - \cos^2 \Delta} \quad , \tag{80}$$

where $\hat{J}_I$ and $\hat{J}_T$ are obtained by substituting the appropriate elements of the initial and target orbits, respectively, into Equation (75). If $\sin \Delta = 0$, then λ_I and λ_T will be measured from a reference defined by the unit vector

$$\hat{N} = \hat{U}_I \quad . \tag{81}$$

If $\sin \Delta \neq 0$, then the unit vector

$$\hat{N} = \left(\hat{J}_T \times \hat{J}_I \right) / \sin \Delta \tag{82}$$

defines the direction of the initial orbit's ascending node on the target orbit plane. This is the reference for measuring λ_I and λ_T when IREF = 1. When IREF = 0, then the "nearly coplanar" convention is to be used and it is necessary to test the sign of the third component of the vector defined by Equation (82). If this component is negative, then Equation (82) has defined the southerly relative node, and the sign of all three components of $\hat{N}$ must be reversed (thereby defining the northerly node) before proceeding with the rest of the calculations.

Now, it is necessary to compute the triad of unit vectors $\left(\hat{i}_o, \hat{j}_o, \hat{k}_o \right)$ which define the local vertical coordinate system at the constrained impulse point. These are given by the equations

$$\hat{k}_o = \left(\hat{J}_I \times \hat{N} \right) \sin \underline{\overline{X}} - \hat{N} \cos \underline{\overline{X}} \quad , \tag{83}$$

$$\hat{j}_o = \hat{J}_I \quad , \tag{84}$$

and

$$\hat{i}_o = \hat{J}_I \times \hat{k}_o \quad , \tag{85}$$

where, of course, the scan control variable $\overline{X}$ represents λ_I for IREF = 1 or 2. The sine and cosine of the true anomaly in the initial orbit at the constrained impulse point can then be obtained from the equations

$$\sin f_o = \hat{k}_o \times \hat{K}_I \cdot \hat{J}_I \tag{86}$$

and

$$\cos f_o = \hat{k}_o \cdot \hat{K}_I \quad . \tag{87}$$

The position and velocity vectors at the constrained impulse point are then given by

$$\vec{r}_o = - \hat{k}_o \, r_o \tag{88}$$

and

$$\vec{v}_o = \sqrt{\mu/p_I} \left[\hat{I}_I \, (e_I + \cos f_o) + \hat{K}_I \sin f_o \right] \quad , \tag{89}$$

where

$$r_o = p_I/(1 + e_I \cos f_o) \quad . \tag{90}$$

The local vertical components of $\vec{v}_o$ are given by the equations

$$\dot{X}_o = \vec{v}_o \cdot \hat{i}_o \tag{91}$$

and

$$\dot{Z}_o = \vec{v}_o \cdot \hat{k}_o \quad . \tag{92}$$

When ISET = 1, then of course it follows from Table 1 that

$$\sin W_I = \sin \underline{Y} \tag{93}$$

and

$$\cos W_I = \cos \underline{Y} \quad . \tag{94}$$

The equation

$$\hat{J}_X = \hat{j}_o \cos W_I - \hat{i}_o \sin W_I \tag{95}$$

defines a unit vector which points in a direction opposite to that of the transfer orbit's angular momentum vector. The cosine of the wedge angle at the unconstrained impulse point then can be obtained from the equation

$$\cos W_T = \hat{J}_T \cdot \hat{J}_X \quad . \tag{96}$$

A trial value for the sine of this angle (whose sign may have to be reversed, depending on the results of subsequent tests) is then computed by use of the equation

$$\sin W_T = \sqrt{1 - \cos^2 W_T} \quad . \tag{97}$$

If $\sin W_T = 0$, then there is a manifold ambiguity regarding the location of the unconstrained impulse, which is resolved arbitrarily by setting

$$\hat{k}_F = - H \hat{k}_o \quad , \tag{98}$$

where H is the auxiliary input variable (described in Section 3.2.2) which must have the value + 1.0 or - 1.0. The unit vector $\hat{k}_F$ points in a direction opposite to that of the position vector at the "free" (i.e., unconstrained) impulse point.

If Equation (97) yields a value of sin $W_T \neq 0$, then a trial value of $\hat{k}_F$ is computed from the equation

$$\hat{k}_F = \left(\hat{J}_T \times \hat{J}_X \right) / \sin W_T \quad . \tag{99}$$

If the quantity $H.\left(\hat{k}_o \cdot \hat{k}_F \right)$ is negative, then the signs of all three components of $\hat{k}_F$ and the sign of sin W_T must be reversed before continuing the calculations.

Having fixed the values of sin W_T and $\hat{k}_F$, the remaining two unit vectors of the local vertical triad at the unconstrained impulse point are obtained from

$$\hat{j}_F = \hat{J}_T \tag{100}$$

and

$$\hat{i}_F = \hat{j}_F \times \hat{k}_F \quad , \tag{101}$$

and the sine and cosine of the true anomaly in the target orbit are obtained from the equations

$$\sin f_F = \hat{k}_F \times \hat{K}_T \cdot \hat{J}_T \tag{102}$$

and

$$\cos f = \hat{k}_F \cdot \hat{K}_T \quad . \tag{103}$$

The position and velocity vectors in the target orbit are given by

$$\vec{r}_F = - \hat{k}_F \, r_F \tag{104}$$

and

$$\vec{v}_F = \sqrt{\mu / p_T} \left[\hat{I}_T \left(e_T + \cos f_F \right) + \hat{K}_T \sin f_F \right] \quad , \tag{105}$$

where

$$r_F = p_T/(1 + e_T \cos f_F) \quad . \tag{106}$$

The local vertical components of $\vec{v}_F$ are obtained from the equations

$$\dot{X}_F = \vec{v}_F \cdot \hat{i}_F \tag{107}$$

and

$$\dot{Z}_F = \vec{v}_F \cdot \hat{k}_F \quad . \tag{108}$$

Finally for the case where ISET = 1, the sine and cosine of the transfer angle are given by

$$\sin \theta = \hat{k}_F \times \hat{k}_o \cdot \hat{J}_X \tag{109}$$

and

$$\cos \theta = \hat{k}_F \cdot \hat{k}_o \quad . \tag{110}$$

When ISET = 2, then $\underline{Y} = \lambda_T$ and the value of $\hat{k}_F$ is given unambiguously by the equation

$$\hat{k}_F = \left(\hat{J}_T \times \hat{N} \right) \sin \underline{Y} - \hat{N} \cos \underline{Y} \quad . \tag{111}$$

The values of $\hat{j}_F$, $\hat{i}_F$, $\sin f_F$, $\cos f_F$, $\vec{r}_F$, $\vec{v}_F$, r_F, $\dot{X}_F$, and $\dot{Z}_F$ can then be obtained from Equations (100) through (108), and the value of $\cos \theta$ from Equation (110). A trial value of $\sin \theta$ is computed by use of the equation

$$\sin \theta = \sqrt{1 - \cos^2 \theta} \quad . \tag{112}$$

If $\sin\theta = 0$, there is a manifold ambiguity regarding the direction of the transfer orbit's angular momentum vector, which is resolved arbitrarily by setting

$$\hat{J}_X = - H \hat{J}_I \quad . \tag{113}$$

If $\sin\theta \neq 0$, then a trial value of $\hat{J}_X$ is computed by using the equation

$$\hat{J}_X = \left(\hat{k}_F \times \hat{k}_o \right) / \sin\theta \quad . \tag{114}$$

If the quantity $H \left(\hat{J}_I \cdot \hat{J}_X \right)$ is greater than zero, then the signs of $\sin\theta$ and all three components of $\hat{J}_X$ must be reversed before continuing the calculations.

After having fixed the values of $\sin\theta$ and $\hat{J}_X$, the sines and cosines of the wedge angles are computed from the equations

$$\sin W_I = \hat{J}_I \times \hat{J}_X \cdot \hat{k}_o \quad , \tag{115}$$

$$\cos W_I = \hat{J}_I \cdot \hat{J}_X \quad , \tag{116}$$

$$\sin W_T = \hat{J}_T \times \hat{J}_X \cdot \hat{k}_F \quad , \tag{117}$$

and

$$\cos W_T = \hat{J}_T \cdot \hat{J}_X \quad . \tag{118}$$

3.2.4 Calculation of the Transfer Orbit Velocity Vector at the Constrained Impulse Point

As in the last section, only the case where the ΔV constraint is applied to the initial impulse will be addressed specifically here. The logic and equations for the other case (where the ΔV constraint is applied to the final impulse) can be obtained by changing the sign of θ and interchanging

the subscripts I and T, the words "initial" and "target," and the words "premaneuver" and "postmaneuver," wherever they appear in the following discussion.

For the purposes of calculating the transfer orbit, it is convenient to rotate the local vertical coordinates at the constrained impulse point through the wedge angle W_I as illustrated in Figure 9, by means of the transformation equations

$$T = X \cos W_I + Y \sin W_I \quad , \tag{119}$$

$$S = - X \sin W_I + Y \cos W_I \quad , \tag{120}$$

and

$$R = - Z \quad . \tag{121}$$

The R and T axes lie in the transfer orbit plane, and the S axis is perpendicular to it. The inverse transformation is defined by the equations

$$X = - S \sin W_I + T \cos W_I \quad , \tag{122}$$

$$Y = S \cos W_I + T \sin W_I \quad , \tag{123}$$

and

$$Z = - R \quad . \tag{124}$$

In the rotated coordinate system, the postmaneuver velocity coordinates are designated $\dot{R}$, $\dot{S}$, and $\dot{T}$, and the equation of the SRM capability sphere takes the form

$$(\dot{R} - \dot{R}_o)^2 + (\dot{S} - \dot{S}_o)^2 + (\dot{T} - \dot{T}_o)^2 = V^2 \quad , \tag{125}$$

which is equivalent to Equation (5) with

$$\dot{R}_o = - \dot{Z}_o \quad , \tag{126}$$

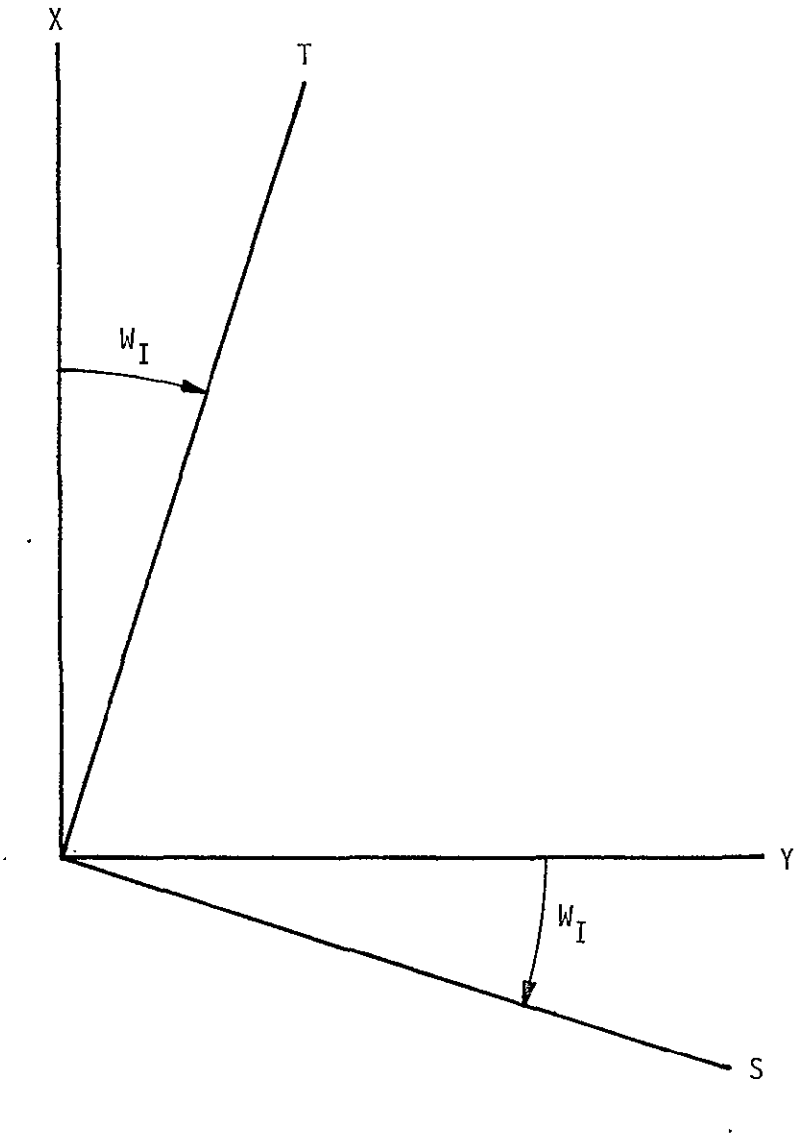

Figure 9. Rotation of Local Vertical Coordinates into Transfer Orbit Plane

$$\dot{S}_o = - \dot{X}_o \sin W_I \quad , \tag{127}$$

and

$$\dot{T}_o = \dot{X}_o \cos W_I \quad . \tag{128}$$

If $V^2 < \dot{S}_o^2$, then the capability sphere does not intersect the required transfer orbit plane, and no solution is possible. If $V^2 > \dot{S}_o^2$, then the capability sphere does intersect the required transfer orbit plane to form a circle in velocity space which is defined by the equations

$$\dot{S} = 0 \tag{129}$$

$$\left(\dot{R} - \dot{R}_o \right)^2 + \left(\dot{T} - \dot{T}_o \right)^2 = V^2 - \dot{S}_o^2 \quad . \tag{130}$$

The existence of a solution depends on whether or not this circle intersects a hyperbola, also lying in the transfer orbit plane, whose equation is to be developed shortly.

Figure 10 is a combined position and velocity vector diagram pertaining to the problem at hand. The equations for calculating the transfer angle θ and the two position vectors $\vec{r}_o$ and $\vec{r}_F$ were defined in Section 3.2.3. The chord vector $\vec{c}$ can be expressed as

$$\vec{c} = \hat{c}\, c \quad , \tag{131}$$

where

$$c = \left| \vec{r}_F - \vec{r}_o \right| \tag{132}$$

and

$$\hat{c} = \left(\vec{r}_F - \vec{r}_o \right) / c \quad . \tag{133}$$

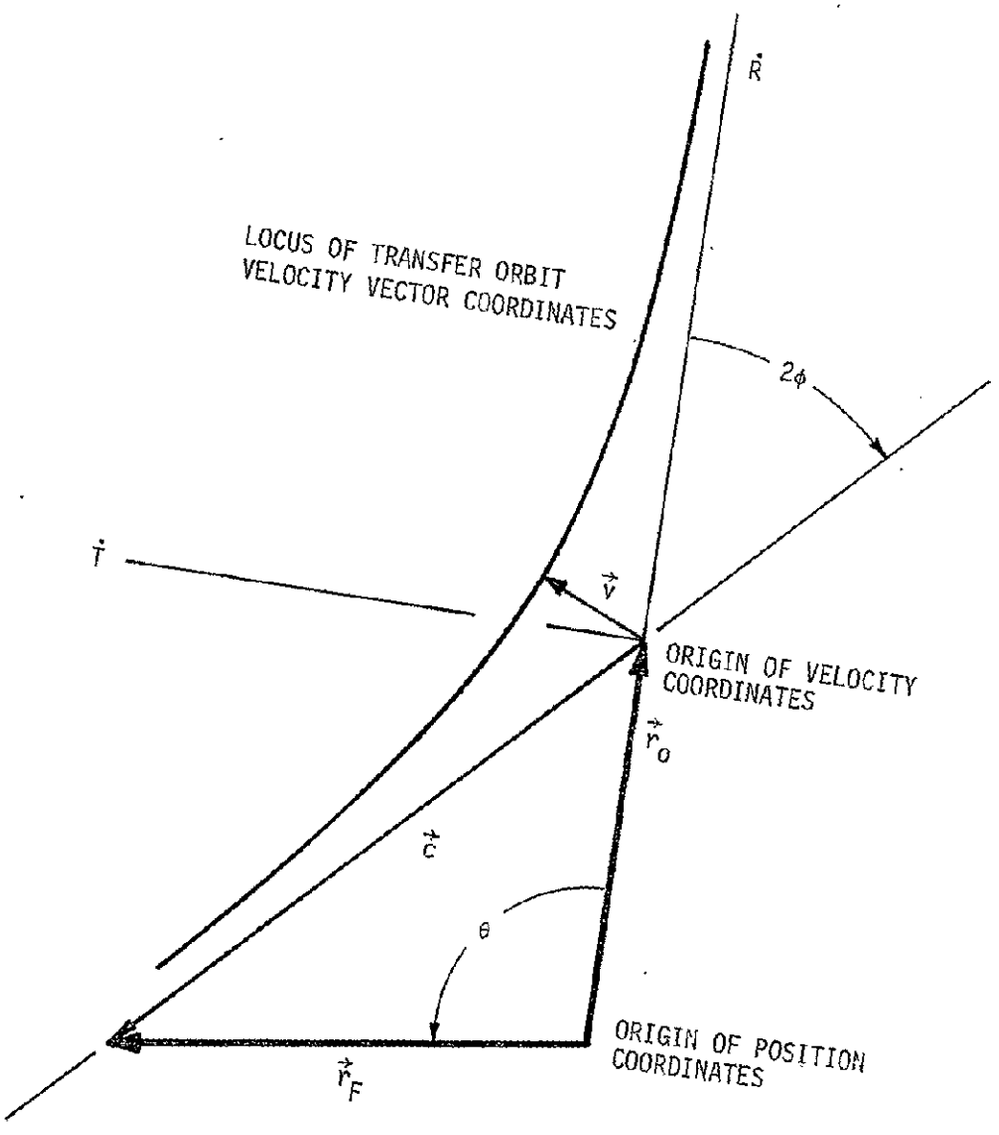

Figure 10. Vector Diagram of Orbital Transfer Problem

The sine and cosine of the angle 2ϕ, which will be used later, can then be obtained from the equations

$$\sin 2\phi = \hat{k}_o \times \hat{c} \cdot \hat{J}_X \qquad (133)$$

and

$$\cos 2\phi = \hat{k}_o \cdot \hat{c} \quad , \qquad (134)$$

where, again, the equations for $\hat{k}_o$ and $\hat{J}_X$ were defined in Section 3.2.3.

Battin has shown (Reference 5, pp. 104-107) that in general the locus of coordinates for all possible transfer orbit velocity vectors (i.e., those velocity vectors which, if supplied to a spacecraft at position $\vec{r}_o$, would cause its orbit to pass through the position $\vec{r}_F$) is a hyperbola whose asymptotes coincide with the chord vector $\vec{c}$ and with the extension of the position vector $\vec{r}_o$. The equation of this hyperbola can be developed from the equation for the semilatus rectum of the transfer orbit

$$p_X = (\dot{T}\, r_o)^2/\mu \qquad (135)$$

and the polar equation

$$\frac{p_X}{r_o} = \frac{\dot{T}\, r_F\, (1 - \cos\theta)}{\dot{T}\, r_o - \dot{T}\, r_F \cos\theta + \dot{R}\, r_F \sin\theta} \qquad (136)$$

from Reference 6. Equations (135) and (136) can be combined and rearranged to yield

$$\dot{T}^2 \left(r_o^{\,2} - r_o\, r_F \cos\theta \right) + \dot{T}\, \dot{R}\, r_o\, r_F \sin\theta = \mu\, r_F\, (1 - \cos\theta) \quad . \qquad (137)$$

The law of sines and the law of cosines, applied to the triangle shown in Figure 10, yields

$$\sin\theta = (c/r_F) \sin 2\phi \qquad (138)$$

and

$$- r_o r_F \cos \theta = \left(c^2 - r_o^2 - r_F^2 \right)/2 \quad , \tag{139}$$

which can be substituted into Equation (137) to obtain

$$\dot{T}^2 \left[\left(c^2 + r_o^2 - r_F^2 \right)/2 \right] + \dot{T} \dot{R} c r_o \sin 2\phi = \mu r_F (1 - \cos \theta) \quad . \tag{140}$$

From the law of cosines we also obtain

$$\left(c^2 + r_o^2 - r_F^2 \right)/2 = c r_o \cos 2\phi \tag{141}$$

which produces

$$\dot{T}^2 \cos 2\phi + \dot{T} \dot{R} \sin 2\phi = (\mu/r_o)(r_F/c)(1 - \cos \theta) \tag{142}$$

when substituted into Equation (140).

Now we rotate the R - T coordinate axes through the angle ϕ as illustrated in Figure 11 by use of the transformation equations

$$\rho = R \cos \phi - T \sin \phi \quad , \tag{143}$$

and

$$\tau = R \sin \phi + T \cos \phi \quad . \tag{144}$$

The inverse transformation equations

$$R = \rho \cos \phi + \tau \sin \phi \quad , \tag{145}$$

and

$$T = - \rho \sin \phi + \tau \cos \phi \quad , \tag{146}$$

when applied to Equation (142), produce

$$\dot{\tau}^2 \cos^2 \phi - \dot{\rho}^2 \sin^2 \phi = (\mu/r_o)(r_F/c)(1 - \cos \theta) \tag{147}$$

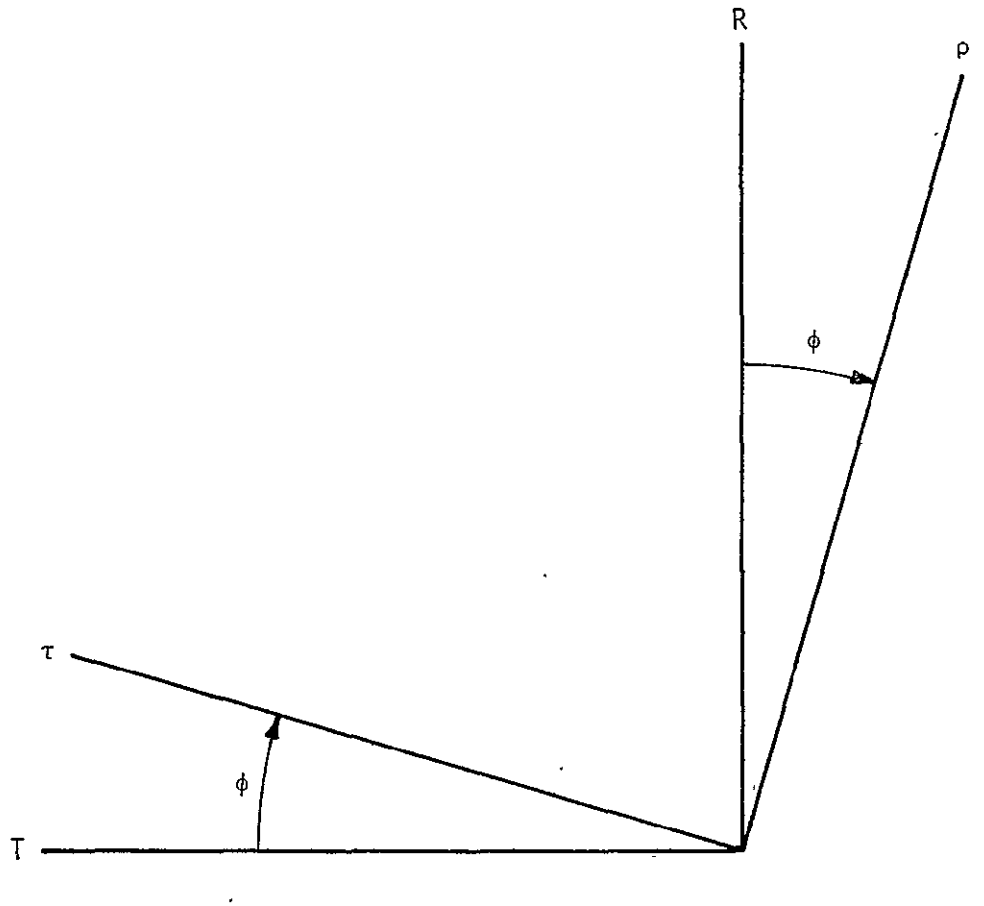

Figure 11. Rotation of Local Vertical Coordinates Through the Angle ϕ

after some algebraic manipulation and the substitution of appropriate trigonometric identities.

The right hand side of Equation (147) is always greater than zero except for the very special case where $\cos\theta = 1$. Such a case is of little practical interest since it involves vertical rectilinear motion in the transfer orbit. Therefore, for our purposes we will assume that no solution exists when $\cos\theta = 1$. When $\cos\theta \neq 1$, Equation (147) can be written in the form

$$\frac{\dot{\tau}^2 \cos^2\phi}{(\mu/r_0)(r_F/c)(1 - \cos\theta)} - \frac{\dot{\rho}^2 \sin^2\phi}{(\mu/r_0)(r_F/c)(1 - \cos\theta)} = 1 \qquad (148)$$

which can be recognized as the equation of a hyperbola whose center lies at the origin of coordinates and whose major axis coincides with the τ-axis.

Now we return to Equation (130), or rather to its equivalent in the $\rho - \tau$ coordinate system, which is

$$(\dot{\rho} - \dot{\rho}_0)^2 + (\dot{\tau} - \dot{\tau}_0)^2 = V^2 - \dot{S}_0^2 \qquad (149)$$

where

$$\dot{\rho}_0 = \dot{R}_0 \cos\phi - \dot{T}_0 \sin\phi \qquad (150)$$

and

$$\dot{\tau}_0 = \dot{R}_0 \sin\phi + \dot{T}_0 \cos\phi \quad . \qquad (151)$$

The solutions to the singly-constrained orbital transfer problem (if any such exist) must satisfy Equations (147) and (149) simultaneously.

For the special case where $\sin\phi = 0$ (which occurs when $\theta = 180°$), Equation (147) yields immediately

$$\dot{\tau} = \sqrt{(\mu/r_0)(r_F/c)(1 - \cos\theta)} \quad . \qquad (152)$$

There is no ambiguity regarding the sign of $\dot{\tau}$. It must be positive; otherwise the direction of the transfer orbit's angular momentum vector (which, at this point, has already been fixed by the equations in Section 3.2.3) would be reversed. The numerical value obtained from Equation (152) can be substituted into Equation (149) to obtain the two solutions

$$\dot{\rho}_{\ell} = \dot{\rho}_0 \pm \sqrt{V^2 - \dot{S}_0^2 - \left(\dot{\tau} - \dot{\tau}_0 \right)^2} \qquad (153)^*$$

where ℓ takes on the value 1 when the minus sign is used in Equation (153) and the value 2 when the plus sign is used.

A value of $\cos \phi = 0$ can occur only if $\cos \theta = 1$, in which case we have already decided to assume that no solution exists for the targeting problem. For the more general case where neither $\sin \phi$ nor $\cos \phi$ is equal to zero, the expression

$$\dot{\tau}^2 = \dot{\rho}^2 \tan^2 \phi + (\mu/r_0)(r_F/c)(1 - \cos \theta)(1 + \tan^2 \phi) \qquad (154)$$

can be obtained from Equation (147) and substituted into Equation (149) to produce the equation

$$2 \dot{\tau}_0 \dot{\tau} = \dot{\rho}^2 (1 + \tan^2 \phi) - 2\dot{\rho}_0 \dot{\rho} + Q_4 \qquad (155)$$

where

$$Q_4 = \dot{\rho}_0^2 + \dot{S}_0^2 + \dot{\tau}_0^2 - V^2 + (\mu/r_0)(r_F/c)(1 - \cos \theta)(1 + \tan^2 \phi) \quad . \qquad (156)$$

If $\dot{\tau}_0 = 0$, then Equation (155) reduces to the quadratic form

$$\dot{\rho}^2 (1 + \tan^2 \phi) - 2\dot{\rho}_0 \dot{\rho} + Q_4 = 0 \qquad (157)$$

---

*If the radicand is negative in Equation (153), then of course there is no real solution to the targeting problem.

which has the roots

$$\dot{\rho}_{\ell} = \frac{\dot{\rho}_o \pm \sqrt{\dot{\rho}_o^2 - Q_4 (1 + \tan^2 \phi)}}{(1 + \tan^2 \phi)} \tag{158}$$

where ℓ is assigned the value 1 when the minus sign is used in Equation (158) and the value 2 when the plus sign is used. If the roots of Equation (157) are real, then they can be substituted into Equation (154) to obtain

$$\dot{\tau}_{\ell} = \sqrt{\dot{\rho}_{\ell}^2 \tan^2 \phi + (\mu/r_o)(r_F/c)(1 - \cos \theta)(1 + \tan^2 \phi)} \tag{159}$$

where, again, $\dot{\tau}_{\ell}$ must be positive to maintain the proper direction of the angular momentum vector.

If $\dot{\tau}_o \neq 0$, then both sides of Equation (155) are squared, and Equation (154) is again substituted into the result to obtain the quartic equation

$$D_1 \dot{\rho}^4 + D_2 \dot{\rho}^3 + D_3 \dot{\rho}^2 + D_4 \dot{\rho} + D_5 = 0 \quad , \tag{160}$$

where

$$D_1 = (1 + \tan^2 \phi)^2 \quad , \tag{161}$$

$$D_2 = - 4\dot{\rho}_o (1 + \tan^2 \phi) \quad , \tag{162}$$

$$D_3 = 4\dot{\rho}_o^2 + 2Q_4 (1 + \tan^2 \phi) - 4\dot{\tau}_o^2 \tan^2 \phi \quad , \tag{163}$$

$$D_4 = - 4Q_4 \dot{\rho}_o \quad , \tag{164}$$

and

$$D_5 = Q_4^2 - 4\dot{\tau}_o^2 (\mu/r_o)(r_F/c)(1 - \cos \theta)(1 + \tan^2 \phi) \quad . \tag{165}$$

Of course, there may be 0, 2, or 4 real roots of Equation (160). Their values (if they exist) can be found by using an explicit algorithm for solving a quartic equation. If the real roots are designated $\dot{\rho}_\ell$, then the corresponding values $\dot{\tau}_\ell$ can be obtained from Equation (155), thus:

$$\dot{\tau}_\ell = \frac{\dot{\rho}_\ell^2 \, (1 + \tan^2 \phi) - 2\dot{\rho}_0 \, \dot{\rho}_\ell + Q_4}{2\dot{\tau}_0} \quad . \tag{166}$$

Again, negative values for $\dot{\tau}_\ell$ are unacceptable and must be rejected along with the root $\dot{\rho}_\ell$ that produced the negative value when substituted into Equation (166).

3.2.5 Designation of the Desired Solution and Calculation of the Transfer Orbit Parameters

In the preceding section we have seen that there may be as many as four distinct real solutions characterized by transfer orbit velocity coordinate pairs $(\dot{\rho}_\ell, \dot{\tau}_\ell)$ at the constrained impulse point, where the subscript ℓ can have the value 1, 2, 3, or 4. It has already been pointed out that $\dot{\tau}_\ell$ must be positive in order to preserve the proper direction of the angular momentum vector. In addition, it is necessary that $\dot{\rho}_\ell^2 + \dot{\tau}_\ell^2 < (2\mu/r_0)$ whenever ISET = 1 or 2 and $\dot{\rho}_\ell > 0$ or whenever ISET = 3 or 4 and $\dot{\rho}_\ell < 0$. This latter restriction is necessary to insure that the transfer orbit, extended in the appropriate direction of motion, will actually pass through the position defined by $\vec{r}_F$.

To obtain a unique solution from the logic described in Section 3.2.4, it is necessary for the trajectory designer to assign an integer value between 1 and 4 to an input flag N to designate the particular solution that he desires. The value of N must remain constant during any particular scanning operation or iterative targeting process, and the selection procedure within the analytic solution logic must be such that the output data generated by a fixed value of N will vary continuously (at least as nearly as possible) as functions of the scan control variables $\overline{X}$ and $\overline{Y}$. This probably can best be accomplished by ordering all of the acceptable coordinate pairs $(\dot{\rho}_n, \dot{\tau}_n)$ such that $\dot{\rho}_{n-1} \leq \dot{\rho}_n \leq \dot{\rho}_{n+1}$ when ISET = 1 or 2 and such that $\dot{\rho}_{n-1} \geq \dot{\rho}_n \geq \dot{\rho}_{n+1}$ when ISET = 3 or 4. This has the effect of

ordering the acceptable solutions such that $\Delta t_{n-1} \leq \Delta t_n \leq \Delta t_{n+1}$, where Δt is the flight time which must be spent in the transfer orbit. If there is an Nth solution in the ordered set, then it should be used to generate the output data. Otherwise, a "no solution" flag should be set to indicate the non-existence of the Nth solution, and further computations should be bypassed.

If the Nth solution does exist, then the local vertical velocity components ($\dot{R}$, $\dot{T}$) in the associated transfer orbit at the constrained impulse point can be calculated by substituting $\dot{\rho}_N$ and $\dot{\tau}_N$ into Equations (145) and (146). The transfer orbit's semilatus rectum p_X can then be obtained from Equation (135), and the eccentricity e_X can be computed from the equation

$$e_X = \sqrt{[(p_X/r_o) - 1]^2 + \dot{R}^2 (p_X/\mu)} \quad . \tag{167}$$

The sine and cosine of the true anomaly in the transfer orbit at the constrained impulse point can be obtained from the equations

$$\sin f_{oX} = \dot{R} \sqrt{(p_X/\mu)} \; / e_X \tag{168}$$

and

$$\cos f_{oX} = [(p_X/r_o) - 1] \; / e_X \quad , \tag{169}$$

provided $e_X \neq 0$. If $e_X = 0$, f_{oX} can be assigned an arbitrary value of zero.

The "local vertical" unit vectors at perigee of the transfer orbit are defined by the equations

$$\hat{I}_X = \left(\hat{J}_X \times \hat{k}_o \right) \cos f_{oX} - \hat{k}_o \sin f_{oX} \tag{170}$$

and

$$\hat{K}_X = \left(\hat{J}_X \times \hat{k}_o \right) \sin f_{ox} + \hat{k}_o \cos f_{oX} \quad . \tag{171}$$

The sine and cosine of the true anomaly in the transfer orbit at the unconstrained maneuver point can be obtained from the equations

$$\sin f_{FX} = \sin f_{oX} \cos \theta \pm \cos f_{oX} \sin \theta \tag{172}$$

and

$$\cos f_{FX} = \cos f_{oX} \cos \theta \mp \sin f_{oX} \sin \theta \quad , \tag{173}$$

where the upper sign is to be used when ISET = 1 or 2 and the lower sign when ISET = 3 or 4. The velocity vector in the transfer orbit at the unconstrained impulse point then can be computed by use of the equation

$$\vec{v}_{FX} = \sqrt{\mu/p_X} \left[\hat{I}_X (e_X + \cos f_{FX}) + \hat{K}_X \sin f_{FX} \right] \quad , \tag{174}$$

which can be used in the equation

$$\Delta V_F = \left| \vec{v}_{FX} - \vec{v}_F \right| \tag{175}$$

to compute the magnitude of the unconstrained velocity increment.

3.3 TWO-IMPULSE ORBITAL TRANSFER WITH PHASING CONSTRAINT

The problem type to be considered in this section is sometimes referred to as the "two-impulse orbital rendezvous problem," since of course to effect a rendezvous it is necessary for the active vehicle to adjust all six of its orbit constants (p, e, i, Ω, ω, t_p) to match those of the target spacecraft. In the true rendezvous problem, where the target is an actual physical object, usually there are a number of very stringent constraints relating to natural lighting conditions at the time of intercept and to the direction and speed of relative motion during the final approach. These constraints do not apply to the general case under consideration here, which more properly might be

thought of as a "phantom rendezvous"* in which the target spacecraft is purely imaginary and therefore incapable of inflicting collision damage on the maneuvering vehicle.

In relation to the targeting problem discussed in Section 3.2, adding an equality constraint on the phasing constant (t_p) of the target orbit has the effect of removing one degree of freedom in the problem solution and drastically reducing the number of possible transfer trajectories. This perhaps can best be illustrated by referring to Figure 10 in Section 3.2.4. If $\vec{r}_0$ is the position of the initial impulse, then the maneuvering vehicle reaches the initial impulse point at a specific time t_0 which is determined† by the phasing constant of the initial orbit. Likewise, the phasing constant of the target orbit determines† the time t_F at which the vehicle must reach the final impulse point defined by $\vec{r}_F$. The flight time in the transfer arc therefore must equal the difference in t_F and t_0. If we restrict the discussion for now to partial-revolution transfer arcs (i.e., where the transfer angle θ is smaller than 360°), then the flight time varies monotonically between zero and infinity along the hyperbolic locus of allowable transfer orbit velocity vector coordinates. It follows that only one discrete point on the hyperbola --- hence only one particular transfer trajectory --- will satisfy the target orbit phasing constraint. In general then, for arbitrarily fixed impulse locations such as illustrated in Figure 10, it is not possible to satisfy a target orbit phasing constraint simultaneously with an equality constraint on the velocity increment magnitude of either (much less both) of the impulses.

There is no explicit solution for calculating the discrete point on the hyperbolic locus that will satisfy the flight time constraint discussed in the previous paragraph. There are a number of efficient iterative algorithms (e.g., Reference 7) for calculating a fixed-flight-time transfer trajectory

*The term "spatial rendezvous" has sometimes been used to distinguish this problem from that of true rendezvous with a physical object; however, the terminology used above is thought to be less ambiguous.

†Subject to discrete variations which are equal to integer multiples of the appropriate orbit period.

from one arbitrary point to another in an inverse-square gravity field. Most of these are based on Lambert's theorem regarding the relationship between flight time, the semimajor axis of the transfer orbit, and the lengths of the sides of the triangle illustrated in Figure 10. For this reason, this particular problem type (where the flight time and the impulse point locations are fixed) is generally characterized as "Lambert's problem" and the solution to such a problem is referred to as a "Lambert solution."

When the initial and final orbits are fully defined (i.e., when p, e, i, Ω, ω, and t_p are known for both orbits) as they are in this case, then the transfer trajectory flight time and the locations of both impulses can be fixed unambiguously by assigning values to the impulse times t_o and t_F. Since it is not possible to satisfy an equality constraint on ΔV at either impulse point when t_o and t_F are assigned arbitrary values, we are reduced to the stratagem of systematically varying (i.e., scanning) the impulse times and computing a Lambert solution for each discrete combination of values in the hope that some particular combinations will produce the desired velocity increment magnitude(s).

The Two-Maneuver Spatial Rendezvous Processor (SR2MAN) of the prototype Mission Design and Analysis Subsystem (MDAS), which is described in Reference 4, is configured to facilitate scanning operations of the type described in the preceding paragraph. In SR2MAN, the scan-control variables consist of one impulse time and a transfer-arc flight time. The specified impulse time may apply either to the first or the second maneuver, and the flight time may be either positive or negative. Based on the sign of the flight time, SR2MAN deduces whether the specified impulse time applies to the first or second maneuver, and computes the time of the other impulse accordingly.

During a scanning operation, the SR2MAN processor is executed repeatedly under the control of the MDAS Monitor Program, according to user-supplied specifications that define the scope and resolution of the scan. The value of the impulse time and the flight time is fixed for each SR2MAN execution. After each execution, the Monitor program stores the SR2MAN output data in an array called a "data box" for subsequent processing, and increments the impulse time and/or the flight time before returning control to SR2MAN so that it can compute a new solution.

Each time it is executed, SR2MAN calculates a value for each of 27 different scalar dependent variables that describe the nature of the transfer trajectory and of the associated maneuvers. After the completion of a scan, all of the output values that were generated during the scan reside in the data box mentioned in the preceding paragraph. Employing the Data Box Display Processor (DBDISP), the MDAS user can create two-dimensional quasi-graphical displays which summarize the behavior of selected dependent variables over the complete scan space. Figure 12 is an example of such a display, where the dependent variables are the magnitudes of the initial and the final velocity increment. Crude contours have been sketched in to illustrate the approximate loci of solutions as they might appear for a particular combination of SRM stage ΔV capabilities. The solution of a singly-constrained or a doubly-constrained problem can be located as accurately as may be necessary (if it exists) by "zooming in" on the appropriate region of the display space in subsequent scans of lesser scope and greater resolution.

If the flight time between the initial and the final impulse is sufficiently great, it may be possible to find multiple solutions to Lambert's problem by allowing the spacecraft to coast through one or more complete revolutions in the transfer orbit. Each complete revolution that is allowed increases the number of possible solutions by two, one of which is characterized by a larger transfer orbit semimajor axis than the other. An integer input variable IXPSOL is used in SR2MAN to determine which solution is desired. A value of 1 designates that the basic partial-rev solution is desired. To obtain a multi-rev solution the user sets IXPSOL = 2 M + L, where M is the number of complete revolutions to be allowed in the transfer orbit and where L has the value 0 or 1 depending on whether the transfer orbit with the larger or the smaller semimajor axis is to be selected. Of course, the value of IXPSOL is always fixed throughout any particular scanning operation.

Although the SR2MAN processor as it is presently configured affords the basic capability (in conjunction with the DBDISP processor) for solving the phantom rendezvous problem as it applies to SRM stages, some modifications are needed to make it fully effective. Using impulse time and flight time as independent variables for scan control produces twofold and manifold

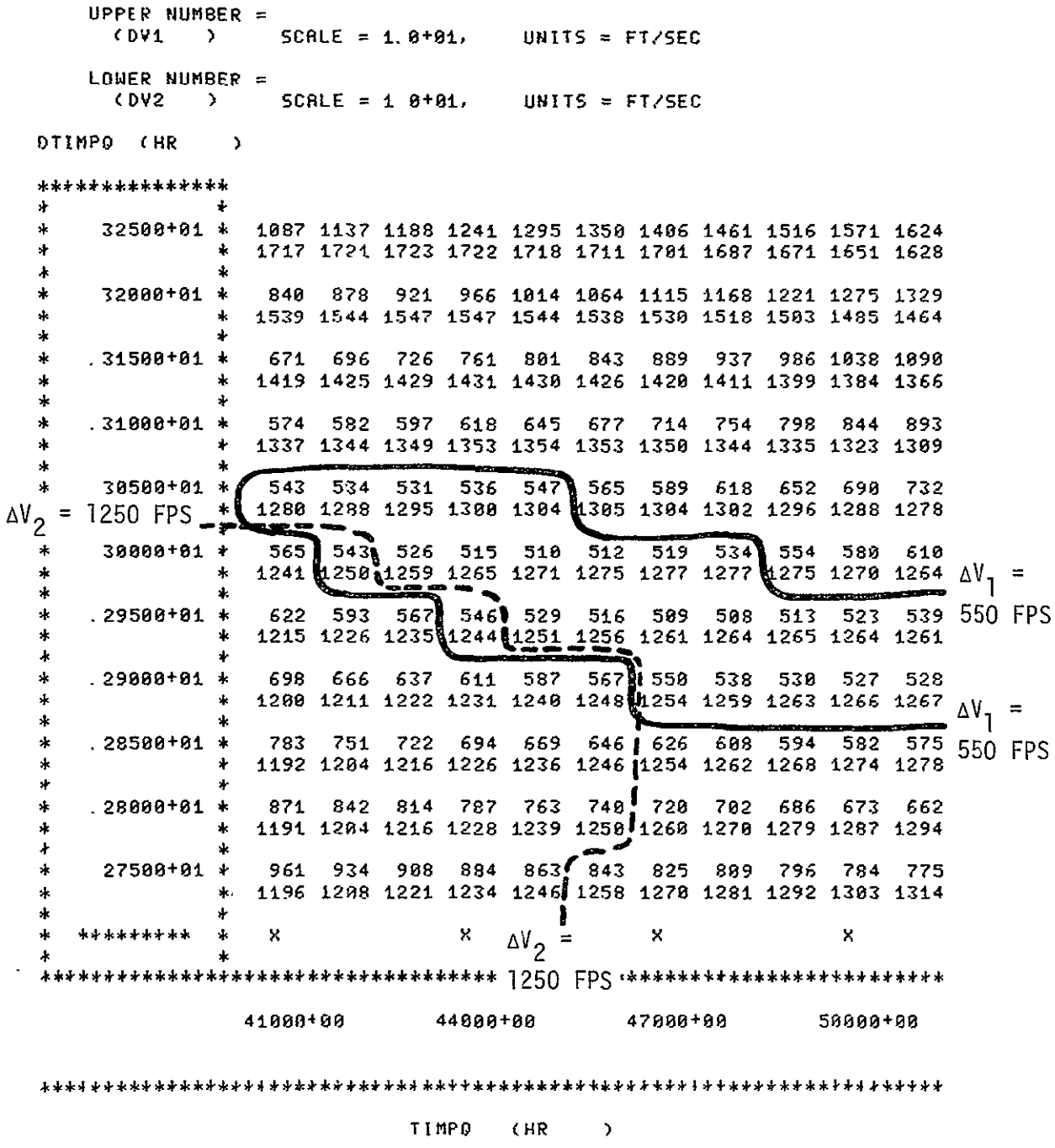

Figure 12. Typical Display Generated by Use of the MDAS SR2MAN and DBDISP Processors

ambiguities regarding the orientation of the transfer orbit angular momentum vector. These ambiguities are essentially the same as those described in Section 3.2.1 for the case where λ_I and λ_T are considered as scan control variables. The SR2MAN logic was formulated originally for use in the design of trajectories for liquid propellant engines, where generally the objective is to minimize the velocity increment magnitudes. Accordingly, within the SR2MAN logic the ambiguities were resolved arbitrarily in favor of smaller ΔV values. An alternate pair of scan-control variables, such as impulse time and wedge angle of the first maneuver, should be provided so that the manifold ambiguity associated with nodal transfers can be resolved fully. An auxiliary input variable (such as the variable H defined in Table 1) should also be provided so that the resolution of the twofold ambiguity that arises in every solution can be controlled externally.

4. RECOMMENDATIONS

The analytic solution for two-impulse orbital transfer without a phasing constraint (Section 3.2) should be given priority with regard to software development. This is the most complicated of the trajectory design problems considered in this report, and probably the one that will have to be solved most frequently in connection with Shuttle payload operations involving solid rocket motors. Preferably the software should be designed, along the same lines as SR2MAN, to operate within the MDAS framework. This will allow the existing MDAS Monitor and the DBDISP processor to be used for scan control and data display.

The SRM targeting requirements for interplanetary injection from a Shuttle parking orbit need to be analyzed in detail. For a given injection point in a fully-defined parking orbit and a specified arrival time at the target planet, all three components of the injection velocity impulse are uniquely determined (subject to very slight variations with varying values of target parameters at the destination planet). Satisfaction of an equality constraint on the magnitude of the velocity increment will therefore be possible only at certain discrete points in the parking orbit. By assuming that $\vec{V}_\infty$ is fixed (which is reasonable for analytical purposes) it appears from a preliminary study of the appropriate equations that an explicit solution for the impulse points might be possible. However, the complexity of such a solution (if it exists) appeared to be such that it would be more properly treated as the subject of a separate report.

Finally, with regard to the algorithms discussed in Section 2.3, a decision regarding possible development of software for simulating SRM powered-flight attitude maneuvers might profitably be delayed until details of the IUS design become more firmly established.

REFERENCES

1. R. E. Phillips, "Final Report - Fuel Depletion Guidance," MIT/CSDL Report No. R-842, September 1974.

2. S. W. Wilson, "Offset Impulse Equations for Finite-Thrust Orbital Maneuvers," TRW IOC No. 6534.3-72-2, 23 October 1972.

3. S. W. Wilson, "Numerical Investigation of Offset Impulse Equations for Fixed-Attitude Finite-Thrust Orbital Maneuvers," TRW IOC No. 6531-3-73-2, 15 March 1973.

4. G. A. Weisskopf, "Functional Capability of the Current Mission-Design-and-Analysis-Subsystem Prototype," JSC Internal Note No. 75-FM-10, 7 February 1975.

5. R. H. Battin, Astronautical Guidance, McGraw-Hill Book Co., New York, 1964.

6. W. Marscher, "A Unified Method of Generating Conic Sections," MIT Report No. R-479, February 1965.

7. R. D. Gilbertson, "Z Iteration Procedure Module (ZIP)," TRW IOC No. 3431.3-16, 14 November 1966.

APPENDIX:

PROBABLE IUS DESIGN CHARACTERISTICS

The following excerpts from Request for Proposal F04701-76-R-0057 (dated 21 January 1976) and its attachments are presented for the purpose of identifying probable design and operational characteristics of the Interim Upper Stage.

A.1 OPERATIONAL PERIOD

"The IUS system segment extends the capability of the Space Shuttle, so that DOD and NASA spacecraft can be delivered beyond low-earth orbits during the 1980-1985 time period." (RFP Attachment 1, p. 1)

A.2 COMPATIBILITY

"The IUS system is primarily to be compatible with the Space Shuttle. However, potential compatibility of the IUS with a Titan booster will be investigated during the validation phase." (RFP, p. 10)

"The IUS vehicle and ASE shall (a) be capable of remaining in the payload bay for a minimum of three orbital periods, and (b) also be compatible with abort, descent, and post landing operations." (RFP Attachment 2, p. 9)

"The IUS vehicle with attached spacecraft should be capable of being deployed from the Orbiter-mounted ASE within 20 minutes, starting at anytime after insertion into the nominal Orbiter parking orbit(s)." (RFP Attachment 2, p. 30)

A.3 OVERALL DESIGN

"The IUS system is to consist of expendable solid propellant stage and appropriate support subsystems." (RFP, p. 9)

"The IUS vehicle comprises the expendable stages that leave the Orbiter and place spacecraft in either extended earth orbits or in planetary mission orbits, in identified configurations suitable for the missions. It includes the stage structure, the solid rocket motors, the reaction control system, the avionics for guidance, navigation and control, telemetry, tracking and command communications, instrumentation, data management equipment, and the required electrical power and electrical cabling. The IUS vehicle also includes the stage to spacecraft interfaces, and the stage to airborne support equipment interfaces." (RFP Attachment 2, p. 7)

"The conceptual design steady-state limit load factor for the IUS vehicle should be limited to -5.0 g's in the longitudinal axis for earth orbital missions. The associated lateral load factors, other than vibrational loads, should be $\pm$ 2.0 g's in the pitch and yaw directions. These total loads shall include thermally induced loads," (RFP Attachment 2, p. 38)

"Conceptual design limit load factors should be limited to -5 g's in the longitudinal axis for earth orbital missions, -10 g's for three-axis stabilized planetary spacecraft, and -15 g's for spinning spacecraft. The associated lateral load factors should be limited to ± 2.0 g's in the pitch and yaw directions. The total load should include thermal induced loads." (RFP Attachment 3, p. 8)

"The IUS system shall provide, by a spin table, the capability to spin spacecraft up to 100 RPM." (RFP Attachment 3, p. 8)

A.4 MAIN PROPULSION

"Propulsion designs shall identify motor family sizes including motor off-loadings, performance parameters, control authority and predicted system life." (RFP Attachment 1, p. 8)

The IUS contractor will be required to determine "the minimum practicable stable of propulsive modules needed to insure operational flexibility in the implementation of the DOD, NASA, and non-NASA mission models." (RFP Attachment 1, p. 13)

Movable nozzles and fixed nozzles with LITVC are to be considered for thrust vector control during SRM design trade studies. (RFP Attachment 6, p. 10)

"The SRM total impulse shall vary by no more than ± TBD per motor." (RFP Attachment 2, p. 49)

A.5 REACTION CONTROL SYSTEM

"RCS operational functions shall include (a) velocity vernier for SRM impulse uncertainty, (b) velocity increments, as for spacecraft post separation maneuvers, (3) single or multi axis attitude maneuvers, (d) coarse or fine mode attitude control, and (e) powered flight roll control." (RFP Attachment 2, p. 49)

Cold gas, monopropellant, and bipropellant systems are to be considered in RCS design trade studies. (RFP Attachment 6, p. 10)

A.6 GUIDANCE, NAVIGATION, AND CONTROL SYSTEM

"The IUS vehicle shall have stable attitude control, about the guidance commanded attitude, for all phases of coast and powered flight operations." (RFP Attachment 2, p. 27)

"The IUS shall be capable of transmitting to the ground: (1) state vector and attitude data at final orbit injection of the IUS vehicle and spacecraft, and..... . The IUS should also be capable of transmitting state vector and attitude data at transfer orbit injection." (RFP Attachment 2, p. 20)

"The SGLS compatible radio links shall be capable of coherent turnaround of PRN modulation used to determine range and range rate at AFSCF ground stations." (RFP Attachment 2, p. 31)

"The STDN compatible radio links shall be capable of coherent turnaround of the side tone ranging used to determine range and range rate at the STDN ground station." (RFP Attachment 3, p. 8)

A.7 PERFORMANCE

The IUS vehicle will be capable of delivering a 5000 pound spacecraft to geosynchronous orbit or a 6000 pound spacecraft to a 12-hour orbit (h_A = 21450 n mi, h_p = 175/350/900 (min/nom/max), i = 63.43°, ω = 270°). (RFP Attachment 2, pp. 24 and 25)

The general position and velocity 3-sigma accuracies* required at geosynchronous orbit injection are given below:

	Position (n mi)	Velocity (fps)
Tangential	± 66	± 16
Normal	± 40	± 12
Radial	± 50	± 75
RSS	± 92	± 78

(RFP Attachment 2, p. 26)

*These are designated as "Guidance and Navigation Accuracies" in the RFP attachment, but considering the context, it is believed that they are intended to represent the total allowable errors at the time of orbit injection.

"The IUS system shall be capable of placing single or multiple spacecraft in orbit by use of a single IUS vehicle in a single Shuttle launch. The IUS shall nominally place the spacecraft at a single orbital location (the spacecraft being required to move to its final location). Relative phasing of the spacecraft shall not be required, except that..... . For multiple deployment, capability for a velocity increment of TBD shall be provided between each spacecraft deployment." (RFP Attachment 2, pp. 8 and 30)

"The IUS vehicle shall be capable of performing maneuvers following separation which prevent direct IUS vehicle plume impingement on the spacecraft and eliminate the possibility of subsequent re-contact with the spacecraft." (RFP Attachment 2, p. 31)

For NASA geosynchronous missions, "The longitudinal placement for synchronous orbit spacecraft shall be $\pm$ 45°." (RFP Attachment 3, p. 6)*

"Ballasting, off-loading, pitch steering and other various energy management techniques should be considered." in motor sizing trade studies. (RFP Attachment 6, p. 10)

*RFP Attachment 3 contains Design Reference Mission specifications for three specific planetary missions and one sun synchronous mission.